nature biomedical engineering

Article

https://doi.org/10.1038/s41551-023-01114-1

Detection of cellular traction forces via the force-triggered Cas12a-mediated catalytic cleavage of a fluorogenic reporter strand

Received: 14 October 2022

Accepted: 26 September 2023

Published online: 13 November 2023

Check for updates

Yuxin Duan[1], Fania Szlam[2], Yuesong Hu[1], Wenchun Chen[3], Renhao Li[3], Yonggang Ke[4], Roman Sniecinski[2] ✉ & Khalid Salaita[1] ✉

Molecular forces generated by cell receptors are infrequent and transient, and hence difficult to detect. Here we report an assay that leverages the CRISPR-associated protein 12a (Cas12a) to amplify the detection of cellular traction forces generated by as few as 50 adherent cells. The assay involves the immobilization of a DNA duplex modified with a ligand specific for a cell receptor. Traction forces of tens of piconewtons trigger the dehybridization of the duplex, exposing a cryptic Cas12-activating strand that sets off the indiscriminate Cas12-mediated cleavage of a fluorogenic reporter strand. We used the assay to perform hundreds of force measurements using human platelets from a single blood draw to extract individualized dose–response curves and half-maximal inhibitory concentrations for a panel of antiplatelet drugs. For seven patients who had undergone cardiopulmonary bypass, platelet dysfunction strongly correlated with the need for platelet transfusion to limit bleeding. The Cas12a-mediated detection of cellular traction forces may be used to assess cell state, and to screen for genes, cell-adhesion ligands, drugs or metabolites that modulate cell mechanics.

The ability of cells to generate mechanical forces is central to a wide range of biological processes, and plays an important role in numerous pathologies[1–4]. Therefore, methods for the quantification of cell-generated forces can be useful in biomedical applications. A central challenge for such methods is that molecular forces that are sensed and transduced by cells are fairly weak, at the scale of piconewtons (pN)[5] and are highly transient and infrequent[6]. We and others recently developed DNA-based tension sensors that respond to cell-generated pN forces and that can be imaged using high-power microscopes with single-molecule sensitivity[7]. Despite the advances in mechanobiology enabled by DNA-tension sensors[3,5,7–9], the use of these probes remains limited because of their weak signal and the need for dedicated microscopy instrumentation. To facilitate mechanobiology studies, it is important to develop facile, robust and sensitive assays that can be broadly adopted.

In biochemistry and molecular biology, a weak or difficult-to-detect signal is typically enhanced by using catalytic amplification reactions (as in polymerase chain reaction (PCR) and enzyme-linked immunosorbent assay). However, these assays have poor compatibility with live-cell measurements. For example, thermal cycling in PCR would destroy most cells. An emerging class of enzymatically amplified reactions that are used in molecular diagnostics are based on clustered regularly interspaced short palindromic repeats (CRISPR) and CRISPR-associated proteins (Cas)[10,11]. One notable Cas enzyme used in diagnostics is CRISPR–Cas12a (Cpf1), which is a class-2 type-V-A enzyme that is loaded with single-stranded guide RNA (gRNA) and is activated upon binding to a complementary single-stranded

[1]Department of Chemistry, Emory University, Atlanta, GA, USA. [2]Department of Anesthesiology, School of Medicine, Emory University, Atlanta, GA, USA. [3]Aflac Cancer and Blood Disorders Center, Children's Healthcare of Atlanta, Departments of Pediatrics, School of Medicine, Emory University, Atlanta, GA, USA. [4]Wallace H. Coulter Department of Biomedical Engineering, Georgia Institute of Technology and Emory University, Atlanta, GA, USA. ✉e-mail: rsnieci@emory.edu; k.salaita@emory.edu

activator DNA. Upon activation of Cas12a, the enzyme undergoes a conformational change that unleashes its indiscriminate cleavage activity (*trans* activity) that hydrolyses any single-stranded DNA (ssDNA) in proximity[12]. The nuclease activity of Cas12a is robust, highly efficient, with $k_{cat}/K_m \approx 10^6$–10^7 M^{-1} s^{-1}, and thus has been used for a number of diagnostic assays for nucleic acid sensing[13] (such as DETECTR[14]) and for metal-ion detection[14,15] Given the sensitivity and specificity of Cas12a-based assays, we were inspired to adopt the Cas12a enzyme to address the limited signal in cellular-tension-sensing assays.

In this Article, specifically, we developed a Mechano-Cas12a Assisted Tension Sensor (MCATS), which is an ultrasensitive fluorescence-based assay for the detection of aggregate number of molecular-force events. In MCATS, the activator is an ssDNA anchored to a surface, such as a glass slide. The activator is concealed by hybridization to a complementary strand that is in turn conjugated to a peptide such as, cyclo-Arg–Gly–Asp–D-Phe–Lys (cRGDfK), or any protein ligand specific to the cell receptor of interest (Fig. 1a,b). When cells are seeded on this surface, surface receptors such as integrins bind to the cRGDfK ligand on the duplex, and apply forces. Forces that exceed the mechanical tolerance of the duplex lead to its rupture, exposing the activator (bottom strand) and thus triggering Cas12a nuclease activity. Upon activation, Cas12a will indiscriminately and catalytically cleave fluorogenic ssDNA reporters. Because Cas12a is highly efficient, its activation generates a massive fluorescence signal output that can be measured using a conventional fluorometer or plate reader for facile and high-throughput readout.

MCATS is a technology that can be applied to study many different types of cell and different biological processes. As a proof-of-concept demonstration, we used MCATS to investigate the forces generated by human platelets because of the importance of mechanical forces in platelet function. Indeed, recent studies using micropatterned polymer structures showed that platelet forces can be used to detect underlying genetic clotting disorders[16], and for predicting trauma-induced coagulopathy[17]. Because MCATS only requires ~5 µl of blood or less to conduct each measurement, a typical blood draw (~5 ml) allows one to run ~1,000 assays in a rapid manner. We leveraged this capability to screen the activity of a panel of clinically approved antiplatelet drugs such as aspirin, eptifibatide, abciximab and ticagrelor. These experiments demonstrate the potential of MCATS for personalized tailoring of anti-coagulant drugs and may help guide therapeutic intervention in the clinic[18]. We also applied MCATS to detect platelet dysfunction following cardiopulmonary bypass (CPB). In a pilot study of seven patients who had undergone CPB, we found that the change in MCATS signal strongly correlated with the need for platelet transfusion. More broadly, MCATS offers an accurate, rapid and cost-efficient method to detect the integrated number of molecular force events generated by cells and will hence open the door to integrating mechanical measurements into the clinic.

Results

Design and optimization of MCATS

We first designed a double-stranded DNA (dsDNA) tension probe that can be mechanically ruptured by cell-generated forces to expose the immobilized activator. The *trans* activity of gRNA–Cas12a nuclease can be activated using two different routes (Fig. 1a)[12]. The first involves a dsDNA that incorporates the protospacer adjacent motif (PAM) sequences. Only dsDNA that is complementary to the gRNA and that incorporates the 4-nt PAM sequence can activate the nuclease. The second route involves an ssDNA sequence that is complementary to the gRNA. The PAM sequence is not required in this case. For MCATS, we designed a PAM-free dsDNA probe, and thus this sequence is unable to activate Cas12a. However, upon mechanical denaturation of this duplex, the bottom strand is exposed, revealing a 20-nt ssDNA domain complementary to the gRNA. Thus, the gRNA/Cas12a complex is exclusively activated as a result of cell-generated forces transmitted to the immobile probe. Active Cas12a then catalytically cleaves fluorogenic single-strand reporter DNA (Fig. 1b,c). The reporter DNA was composed of a short poly T sequence to minimize secondary structure and was tagged with a quencher–fluorophore pair at its termini, such that it was dequenched upon Cas12a hydrolysis. The activator domain is not restricted to the sequence used here and can be designed to tune the force response being detected. The sequences of all oligonucleotides used in this work are provided in Supplementary Table 1.

Given that surface-tethered Cas12a had not been reported in the literature, and the potential for hindered activity due to immobilization[19], we first measured the kinetics of Cas12a when the activator is immobilized on a surface and compared it with reactions where the activator was in solution. In this assay, biotinylated activator (100 nM) was anchored to streptavidin-coated surfaces by incubating for 1 h at room temperature. Based on our previous surface calibration, this procedure generates a DNA density of 1,330 ± 60 molecules μm^{-2} (ref. 20). Next, the gRNA–Cas12a complex (20 nM) and reporter DNA (100 nM) were added to the surface, and a fluorescence plate reader was used to monitor the fluorescence signal in each well of the 96-well plate. The measurement showed that ss-activator triggered the Cas12a nuclease and generated a strong fluorescent response. In contrast, the ds-activator (concealed activator) showed only minimal signal (Fig. 1d).

Next, we tested whether adding a spacer to the activator may boost Cas12a cleavage rates. We tested four activators with different-length polyT spacers of 0, 6, 60 and 160 nt. The surface density calibration showed that 6- and 60-nt polyT spacers reduced surface density only slightly (~18%) while the long 160-nt spacer caused the surface density to decrease to 60% of the 0-nt spacer probe (Extended Data Fig. 1). The apparent initial rate constant (fluorescence signal change between $t = 10$ and 20 min) for these immobilized activators is plotted in Fig. 1e and showed that the apparent initial rate constant was enhanced with longer spacers with the exception for the 160-nt activator. The enhanced activity with longer spacers is probably due to reduced steric hinderance, but this effect is offset by the reduced effective activator density at extreme spacer lengths. Notably, we expect that the Cas12a will release the activator from the surface with suitable length spacers. This is supported by the observation that activator surface density is diminished by 70% for the 60 polyT spacer after 1 h of adding the Cas12a (Extended Data Fig. 2). All subsequent work with MCATS employed the activator with 60-nt polyT spacer due to its superior signal amplification.

To further optimize MCATS, we measured Cas12a activity as a function of assay temperature, buffer and reaction time (Supplementary Fig. 1). The results indicate the Cas12a work best at 37 °C, in cell culture medium with 10 mM of Mg^{2+}. We also compared the signal-to-noise ratio (S/N) of the assay using two reporter oligonucleotides (Supplementary Fig. 2). The reporter strand tagged with Atto565N-BHQ2 shows an approximately two times higher S/N compared with FAM-Iowa black reporter strand because of its better quenching efficiency. Using the optimized conditions, we investigated the limit of detection (LOD) of our assay both for surface-tethered activator as well as soluble activator as a reference (Fig. 1f,g). To tune the activator surface density, we created surfaces composed of a binary mixture of ssDNA activator and the blocked (double-stranded) control DNA. We maintained a total activator solution concentration of 100 nM but tuned the ratio between the blocked DNA and single-stranded activator. We then added Cas12a–gRNA and fluorogenic reporter to the well and measured the final fluorescence intensity after 1 h of enzyme activity. The LOD was then inferred from the ratio of 3.3× standard deviation (s.d.) of the background normalized by the slope of the fluorescence versus concentration plot. The results showed that the LOD for nucleic acid sensing was 95.2 fM in solution and 1,712 molecules mm^{-2} on a surface. This analysis provides the basis for using MCATS to sensitively detect the cumulative number of molecular force events generated by cells.

https://doi.org/10.1038/s41551-023-01114-1

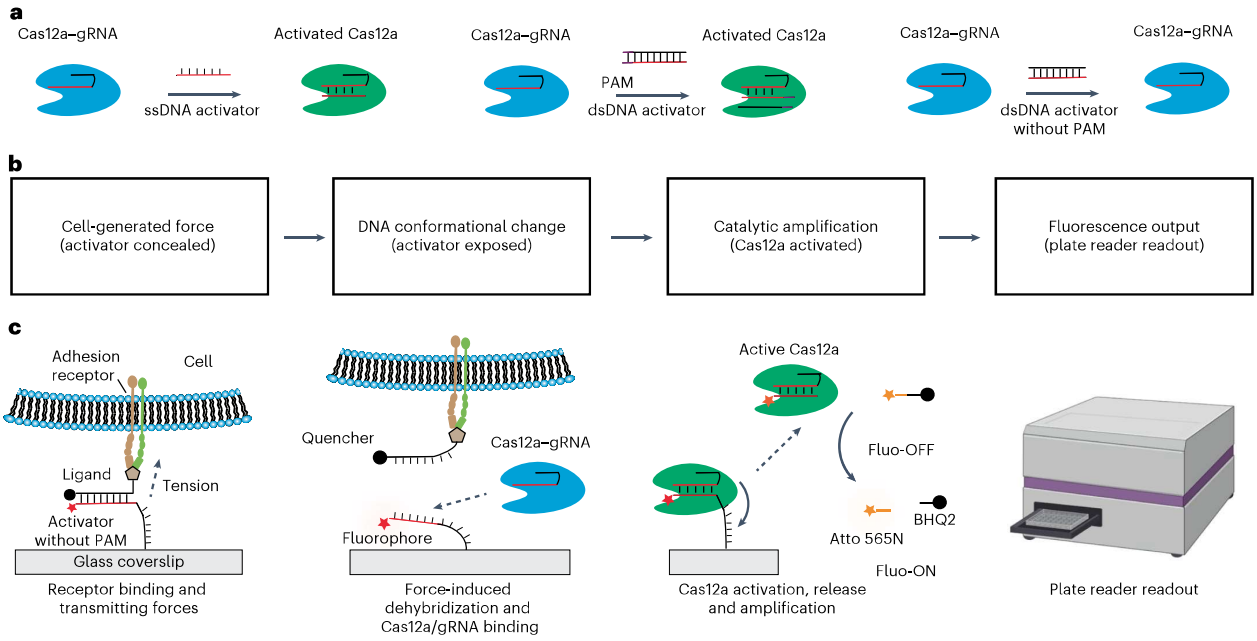

Fig. 1 | Scheme and characterization of MCATS. a, Schematic showing the potential mechanisms of activating Cas12a. **b**, Flow chart depicting MCATS. **c**, Corresponding scheme illustrating MCATS. Molecular traction forces mechanically melt the duplex probe and reveal an activator sequence that triggers Cas12a to cleave reporter strands in solution. The activator was tagged with Atto647N to aid in quantification and validation. **d**, Characterization of Cas12a activity for surface-tethered activators of 0-, 6-, 60- and 160-nt poly T linkers along with negative controls using concealed (duplexed) activators. Plot of time-dependent fluorescence intensity measured using a conventional plate reader. Error bars represent s.e.m. obtained from three independent experiments, and centre of error bars represents mean of the fluorescence intensity (FI). **e**, Plot of Cas12a apparent initial cleavage rate as a function of linker length for immobilized activator. The apparent rate was determined using the change in fluorescence between $t = 10$ min and 20 min. The error bars represent s.e.m. of $n = 3$ independent experiments, and centre of error bars represents mean of the apparent initial rates. **f**, Plot of fluorescence intensity at $t = 1$ h as a function of activator concentration for reactions employing 20 nM Cas12a–gRNA complex and 100 nM reporter DNA. Each reaction also contained 100 nM of dsDNA to mimic the concealed activator. The error bars stand for s.e.m. of $n = 3$ independent experiments. Centre of the error bar represents mean of MCATS measurements from three independent experiments. LOD = 3.3(s.d. of blank/slope of calibration curve) = 95.2 fM. **g**, Plot of fluorescence intensity as a function of surface density of activator. Each reaction contained 20 nM Cas12a–gRNA complex and 100 nM reporter DNA. Surface displayed a binary mixture of activator and scrambled DNA. LOD, 1,712 molecules mm^{-2}. The error bars stand for s.e.m. of $n = 3$ independent experiments. Centre of the error bar represents mean of MCATS measurements from three independent experiments. a.u., arbitrary units.

Rapid, robust, ultrasensitive detection of tension with MCATS

We next applied the MCATS assay to detect integrin-mediated cell traction forces in immortalized cell lines. Integrins are a family of heterodimeric cell surface adhesion receptors that bridge the cellular cytoskeleton with the extracellular matrix to mediate a variety of processes including cell adhesion and migration[2]. Previous research has shown that integrin receptors can apply pN forces that are sufficient to mechanically denature DNA duplexes[21]. Hence, measuring integrin receptor forces with NIH/3T3 cells is an appropriate model to validate the MCATS assay.

As is shown in Fig. 2a, DNA duplexes that present cRGDfK ligand and concealed Cas12a activator were immobilized on the surface. The conjugation of ligand to duplex was achieved via copper(I)-catalysed azide–alkyne cycloaddition and was verified with electrospray ionization (ESI)–mass spectrometry (Supplementary Fig. 3 and Supplementary Table 2). NIH/3T3 fibroblast cells were then seeded on these surfaces for 1 h.

We designed two types of DNA duplex that have identical sequences and thermal melting temperatures, but different geometries and mechanical tolerances (Fig. 2b). When the activator is anchored through its 5′ terminus, the cRGDfK ligand is presented on the 3′ terminus of the top strand. Hence, this probe denatures through an unzipping process that has a lower activation barrier and displays a mechanical rupture threshold of 12 pN. In contrast, when the activator is anchored through its 3′ terminus, the probe denatures by shearing that has a larger mechanical threshold of 56 pN.

The same number of cells (25,000 cells) was incubated on the two types of surface for 1 h before running the Cas12a amplification assay. As expected, we observed an increase in fluorescence signal for both the 12-pN and 56-pN probes (tagged with fluorophore–quencher pairs) due to mechanical denaturation of the duplex (Fig. 2c). As expected, the probes in the unzipping geometry (12 pN) were more significantly denatured compared with shearing mode probes (56 pN), in agreement with past literature (Fig. 2b,c)[22]. We next added the Cas12a and reporter DNA to trigger the MCATS assay for 1 h and then measured bulk fluorescence (λ_{ex} = 540 nm and λ_{em} = 590 nm) using the plate reader (Fig. 2d). Importantly, the 12-pN unzipping mode probes also generated a greater MCATS signal, reflecting the greater density of exposed activator. MCATS produced over 100-fold greater signal compared with previously reported mechanically triggered-hybridization chain reaction assay (mechano-HCR), which confirms that this assay is more sensitive and offers a simplified experimental process as no washing steps are required (Supplementary Fig. 4)[20].

We further validated the MCATS assay by seeding increasing numbers of NIH/3T3 cells in 96-well plates and measuring associated MCATS signal in each well. We observed that increasing cell densities led to greater MCATS signal (Fig. 2e,f). Impressively, we found that MCATS can detect the tension generated from as few as 50 fibroblasts in a 96-well plate using a conventional plate reader (Fig. 2e inset). We further tested whether MCATS can be used to produce a dose–response curve for NIH-3T3 cell incubated with Rho kinase inhibitor, Y-27632, which targets the phosphorylation of myosin light chain and therefore dampens forces transmitted by focal adhesions. We pre-treated NIH/3T3 cells with a range of Y-27632 concentrations (0–50 μM) for 30 min and then ran MCATS with the drug-treated cell. MCATS signal showed a dose-dependent reduction as a function of increasing Y-27632 concentration (Fig. 2g,h), indicating that plate-reader-based MCATS readout can report cell forces modulated by MLC inhibition. By fitting the data to a standard dose–response inhibition function (signal = 100/(1 + [drug]/IC_{50})), we found that the mechano-IC_{50} = 7.9 μM (95% confidence interval 5.5–11.6 μM), which matches previous literature reporting IC_{50} of 5–10 μM (ref. 23).

Given that integrin display is highly heterogeneous across cell types and tissues, we next applied MCATS to measure integrin-subtype-mediated forces in HeLa cells, which express $\alpha_5\beta_1$, $\alpha_V\beta_5$ and $\alpha_V\beta_3$ integrins[24–26]. Moreover, integrin $\alpha_V\beta_3$ levels are correlated with the malignancy potential of tumour cells[27]. To study how specific integrin subtypes mediate differential traction forces, we incubated cells with two different types of monoclonal antibody: anti-$\alpha_5\beta_1$ and anti-$\alpha_V\beta_3$ for 30 min at 10 μg ml^{-1} before running the MCATS assay. The results showed that inhibition of integrin $\alpha_5\beta_1$ and $\alpha_V\beta_3$ led to a significant decrease in MCATS signal on 12-pN probes (Extended Data Fig. 3, P = 0.003 for blocked $\alpha_V\beta_3$ and P = 0.01 for blocked $\alpha_5\beta_1$). However, on 56-pN probes, only inhibition of $\alpha_5\beta_1$ showed a significant decrease in MCATS signal (P = 0.04). The result confirms that $\alpha_5\beta_1$ and $\alpha_V\beta_3$ both contribute to adhesion and traction force generation of HeLa cells. However, $\alpha_5\beta_1$ primarily exerts F > 56 pN, which is consistent with precedent literature indicating greater rupture forces for $\alpha_5\beta_1$ than that of $\alpha_V\beta_3$ (refs. 28,29). These results further validate the versatility of using MCATS for screening integrin-specific force transmission, which may have implications in mechanotyping cancer cell lines.

Measurement of platelet traction forces using MCATS

Platelets are primary cells and are well suited for MCATS analysis because contractile forces are critical in platelet function in forming clots that mechanically resist blood shear flow and seal a wound. Thus, we tested if MCATS can be used to measure platelet traction forces in a high throughput manner (Fig. 3a). We first purified human platelets from blood samples collected in collection tubes containing sodium citrate or EDTA from donors. The sample was then centrifuged for 12 min at 140g (with 0.02 U apyrase) to obtain platelet-rich plasma (PRP). Then platelets were prepared from PRP by centrifugation for 5 min at 700g with 3 μM prostaglandin E1 (PGE-1). The platelets were then resuspended in Tyrodes buffer and centrifuged for 5 min at 700g with 3 μM PGE-1. Finally, platelets were resuspended in Tyrodes buffer. It is worth noting that apyrase is important in the platelet purification process to prevent haemolysis-mediated platelet aggregation (Supplementary Fig. 5). In additional controls, we found that tubes containing either EDTA or citrate will not influence platelet tension after purification (Supplementary Fig. 5).

We first tested MCATS as a function of the number of platelets seeded on the unzipping duplex surfaces. We found that MCATS detected tension signal from as few as 2,000 platelets (Extended Data Fig. 4). We chose 2×10^6 platelets in the following experiments because this concentration of platelets in a 96-well plate offered the strongest signal for the assay. To validate that MCATS response was sensitive to the mechanical tolerance of the probes, we tested platelets that were seeded on DNA tension probes in shearing and unzipping geometries, with thresholds of 56 and 12 pN, respectively. MCATS signal was six-fold greater on the unzipping probes compared with that of the shearing duplex probes, which is consistent with literature precedent by our group and others (Fig. 3b,c)[2,20,30–32]. To better characterize the reproducibility of MCATS, we performed ten measurements on platelets collected from a single healthy donor. As is shown in Fig. 3d, the mean of the measurements was 125,000 ± 14,700 a.u., showing a coefficient of variation of 11.7%. Interestingly, this value is comparable to the CV reported for other US Food and Drug Administration-approved coagulation assays such as Multiplate (~14.4%)[33], VerifyNow (~17.7%)[33] and light transmission aggregometry (LTA) (~5–12%)[34]. Furthermore, we also estimated the day-to-day variance in MCATS signal for two healthy donors (Extended Data Fig. 5). The coefficient variation for the two donors from three independent blood draws was 0.09 and 0.16, which is consistent with the assay variance, indicating that healthy platelet may maintain stable tension levels for many months. However, due to the limited number of donors studied over a fairly short time window, further investigation is needed to better quantify time-dependent changes in platelet mechanical contractility. Taken together, these experiments help reveal MCATS signal variation when testing the same pool of platelets from a single blood draw as well as the variation across multiple blood draws.

https://doi.org/10.1038/s41551-023-01114-1

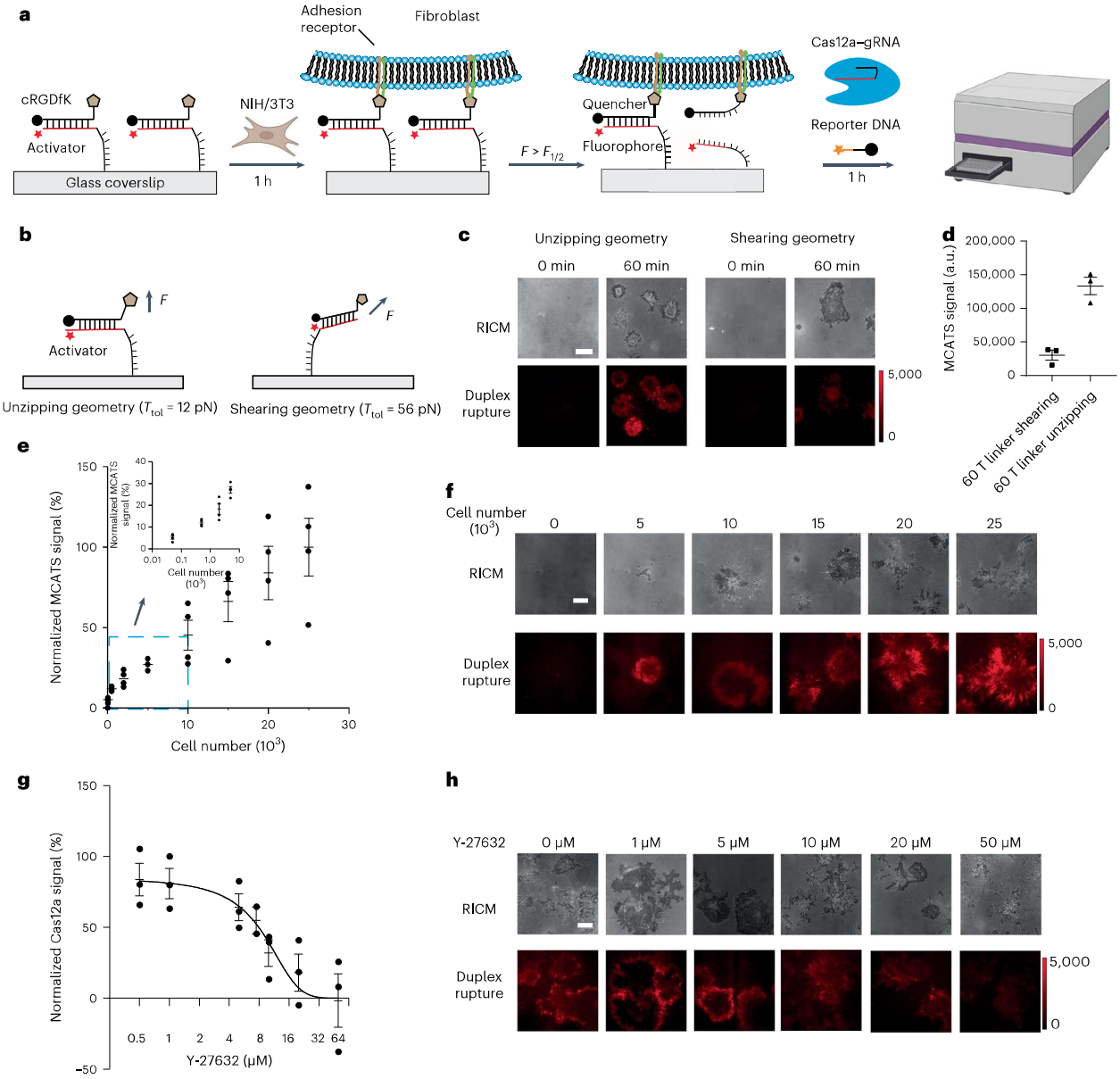

Fig. 2 | MCATS demonstration using fibroblasts. a, Schematic of MCATS assay to study NIH/3T3 integrin-mediated forces. **b**, Schematic comparing designs of concealed activator in shearing and unzipping geometries. **c**, Representative RICM and fluorescence images of cells cultured on unzipping (12 pN) and shearing (56 pN) surfaces at $t = 0$, and 1 h after cell seeding. Scale bar, 12 μm. The fluorescence emission is due to dequenching of Atto647N following top strand denaturation. The intensity bar indicates the absolute range of intensity values for each image. **d**, Plot shows MCATS signal measured using plate reader for cells incubated on $T_{tol} = 12$ pN and $T_{tol} = 56$ pN surfaces. Error bars represent s.e.m. from $n = 3$ independent experiments. Centre of the error bar represents average MCATS measurement of three independent experiments. **e**, Plot showing plate reader measured MCATS signal as a function of the number of cells seeded. Error bar represents s.e.m. from four independent experiments. Centre of the error bar represents average MCATS signal of four independent experiments. Inset shows signal in the regime of low numbers of cells (50–5,000 cells). **f**, Representative RICM and duplex rupture (red) fluorescence images for unzipping probes. Scale bar, 12 μm. **g**, Plot of MCATS signal as a function of Y-27632 concentration. Drug was incubated for 30 min before seeding cells on the surface. Error bar represents s.e.m. from three independent experiments. Centre of the error bar represents mean normalized MCATS signal of three independent experiments. Mechano-IC_{50} was calculated by fitting plot to a standard dose–response function: normalized signal = $100/(1 + [\text{drug}]/IC_{50})$. The values were normalized to the signal obtained from the 25,000 cells per well samples without drug treatment. All measurements were background subtracted using negative control wells lacking cells. **h**, Representative RICM and duplex rupture (red) fluorescence images of drug-treated fibroblasts at $t = 1$ h after seeding. Scale bar, 12 μm.

Another parameter that could influence platelet traction forces is adenosine 5′-diphosphate (ADP) agonist concentration, which is well known to trigger platelet activation and adhesion. We therefore tested the dose–response of platelets to agonist using MCATS and found increasing tension signal as a function of ADP. These results were further validated with LTA, which is commonly used to assess platelet function (Fig. 3e and Extended Data Fig. 6). Aggregometry, however, requires 100-fold greater sample volumes and dedicated

https://doi.org/10.1038/s41551-023-01114-1

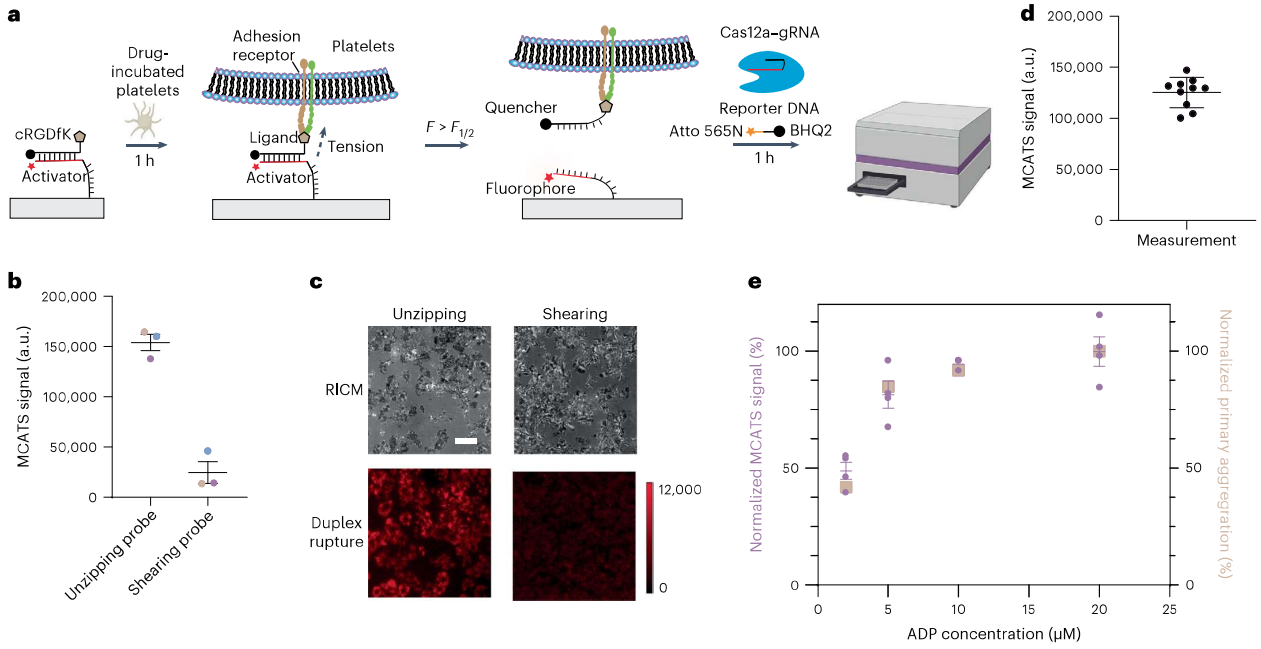

Fig. 3 | MCATS for high-throughput measurement of platelet traction forces. **a**, Schematic showing mechanism of MCATS to quantify platelet-mediated forces. **b**, Bar graph shows MCATS signal of the same number of platelets incubated on T_{tol} = 12 pN and T_{tol} = 56 pN probes. Error bars represent s.e.m. obtained from n = 3 blood draws from three donors, and each was colour coded. The MCATS signal from each unique blood draw was averaged from technical replicates (different wells). **c**, Representative RICM and fluorescence images of cells cultured on T_{tol} = 12 pN and T_{tol} = 56 pN surfaces for 1 h. Scale bar, 12 μm. The red colour is emission from Atto647N tagging the activator. The intensity bar next to each fluorescence image shows the absolute signal intensity for each image. **d**, MCATS reproducibility analysis. The plot shows the MCATS signal of ten independent measurements of the same platelet sample collected from a single blood draw. The black line represents the mean and s.d. of the ten measurements. **e**, Plot of MCATS signal (purple) and primary aggregation (beige) signal obtained from donor platelets upon activating with ADP. Aggregometry data collected from a single donor. MCATS signal is the average from n = 4 donors. The values were normalized to the signal obtained from the wells with 20 μM ADP. Error bar represents s.e.m. from n = 4 donors.

instruments, which shows the advantage of MCATS in assessing platelet function with cellular forces. Other agonists such as thrombin receptor activating peptide and collagen were also tested and showed increasing tension signal as a function of dose of agonist (Supplementary Fig. 6).

High-throughput determination of platelet inhibitors' influence on platelet tension

We next investigated the MCATS signal of human platelets under the influence of different antiplatelet drugs. Antiplatelet agents are some of the most commonly prescribed drugs in the world. Currently, 30 million Americans take antiplatelet medications such as daily aspirin to reduce the risk of cardiovascular events, but ~16.6 of 100 patients experience bleeding as a side effect and 5% are resistant to aspirin[35].

We tested multiple types of US Food and Drug Administration-approved antiplatelet drugs: aspirin, which inhibits the activity of cyclooxygenase (COX), the integrin $\alpha_{IIb}\beta_3$ (also known as GPIIb/IIIa) antagonists eptifibatide, 7E3 (monoclonal antibody) and the P2Y12 inhibitor ticagrelor (Fig. 4a)[36–38]. As is shown in Fig. 4b, aspirin targets COXs 1 and 2 (COX-1 and COX-2), leading to an inhibition of prostaglandin biosynthesis and synthesis of thromboxane A2 (TxA2), which is essential in platelet activation and traction force generation[39]. Integrilin and 7E3 are drugs that selectively bind to $\alpha_{IIb}\beta_3$ integrins and compete with fibrinogen binding[40,41]. Blocking the integrin receptor with either drug dampens outside-in mechanical signal transduction and decreases platelet activation and force transmission. Finally, ticagrelor is an inhibitor of the purine receptor, P2Y12, which is critical in driving platelet activation following ADP binding. P2Y12 is a G-protein coupled receptor that activates PLCb and generates a Ca^{2+} flux that boosts myosin contractility and traction force generation by the platelet[42]. In the drug inhibition experiments, we incubated platelets with different drugs at room temperature for 30 min and plated 2×10^6 treated human platelets in each well for 1 h and then performed MCATS. For all the compounds tested, we observed a dose-dependent decrease in the 12-pN duplex rupture in both microscopy imaging of duplex ruptures as well as MCATS signal that was detected using a plate reader (Fig. 4c–f and Extended Data Fig. 7). All drugs showed a significant drop in signal upon treating platelets. (P value of <0.0001, 0.009, <0.0001 and 0.005 for aspirin, eptifibatide, 7E3 and ticagrelor, respectively) By fitting the plot of MCATS signal with a standard dose–response inhibition function (Signal = Bottom + (Top − Bottom)/(1 + ([drug]/IC_{50}))), we determined the mechano-IC_{50} for aspirin, eptifibatide, 7E3 and ticagrelor for each individual donor and plotted the data in Fig. 4c–f. MCATS was found to be robust as the signal generated from the same blood draw of the same donor was highly consistent ($s \approx 10\%$). However, we found donor-to-donor variability in mechano-IC_{50}, which probably reflects the biological heterogeneity of the drug response especially in aspirin-treated group. Importantly, the values we measured were consistent with literature precedent[41,43–46]. Because each measurement only requires 2×10^6 platelets while 1 ml of blood contains ~10^9 platelets, a typical 5 ml blood draw can be used to run ~2,500 assays, thus opening the door for massive screening to determine drug sensitivity in a personalized manner.

MCATS detects platelet dysfunction and correlates with transfusion need in subjects following CPB

Finally, we investigated whether MCATS can be used to assess platelet dysfunction in patients who had undergone CPB. In a subset of patients (10–23%), CPB leads to severe post-operative bleeding

https://doi.org/10.1038/s41551-023-01114-1

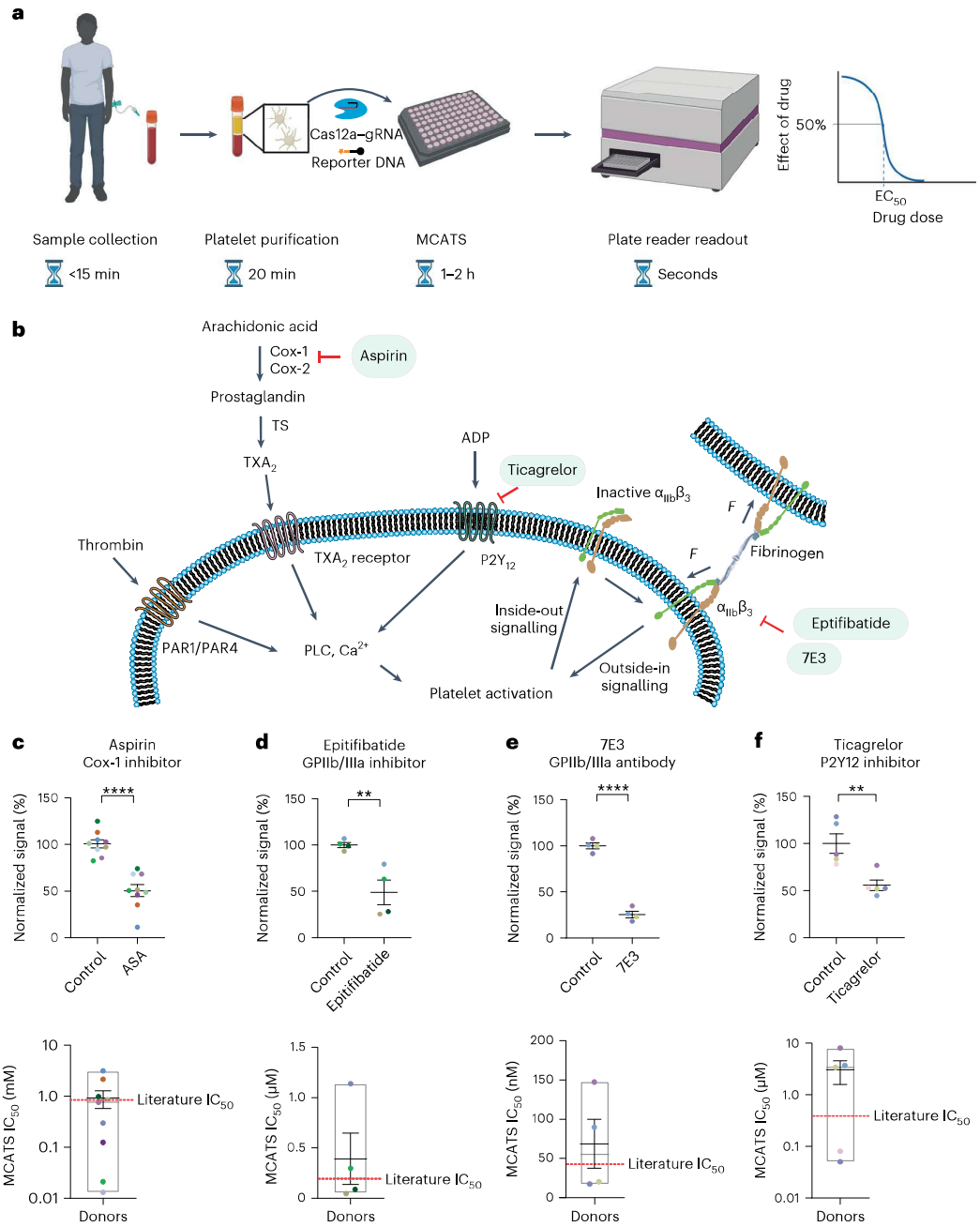

Fig. 4 | MCATS for personalized antiplatelet drug-sensitivity measurement. **a**, Schematic showing overall MCATS workflow using human platelets. Created with BioRender.com. **b**, Mechanism of different antiplatelet drugs inhibiting platelet traction forces. **c**–**f**, Plots of MCATS signal for platelets before and after inhibition using aspirin (0.1 mM, **c**), eptifibatide (1 μM, **d**), 7E3 (10 μg ml^{-1}, **e**) and ticagrelor (1 μM, **f**). Donor platelets were treated with the inhibitor for 30 min at room temperature before performing MCATS. Each data point represents the average of $n = 2$ measurements on different chips from a single donor. Different donors are colour coded. The mean and s.e.m. are shown for each drug treatment. Data were normalized to average of non-treated group. Significance is calculated with two-tailed Student's *t*-tests. *P* values of <0.0001, 0.009, <0.0001 and 0.005 for aspirin, eptifibatide, 7E3 and ticagrelor, respectively. ** and **** represent *P* value < 0.01 and 0.0001, respectively. The bottom set of plots show the mechano-IC_{50} calculated from a dose–response titration of six drug concentrations for each drug for colour-coded individual donors. The MCATS signal at each drug concentration for each donor is obtained from an average of $n = 2$ measurements collected from different chips. Body of the box plots represents first and third quartiles, and red horizontal line represents the literature-reported IC_{50}. Error bars represent s.e.m. for each drug from $n = 9$ donors for aspirin, 4 donors for eptifibatide, 4 donors for 7E3 and 5 donors for ticagrelor. Mechano-IC_{50} was calculated by fitting plot to a standard dose–response function: Signal = Bottom + (Top − Bottom)/(1 + ([drug]/IC_{50})).

requiring blood transfusion[47–49]. Past literature has demonstrated that CPB surgery and other extracorporeal circuits such as extracorporeal membrane oxygenation lead to changes in membrane glycoprotein GPIb-IX-V (ref. 50) as well as integrin activation[51], which results in platelet dysfunction[49]. The likelihood of patient bleeding following CPB is typically assessed using platelet function assays such as impedance aggregometry and thromboelastography (TEG). Despite their widespread use, such assays provide only a weak prediction of severe bleeding. For example, the PLATFORM clinical trial showed that impedance aggregometry has a 40% predictive value for severe bleeding[52], while other studies showed that TEG has a 0.78 area under the curve for predicting post-operative bleeding[53,54], probably because TEG and aggregometry are highly dependent on platelet count, which can bias aggregation dynamics[55]. The ability to anticipate the risk of developing coagulopathy due to platelet dysfunction more accurately is desirable as it could aid in determining the optimal timing of cardiac surgery for patients on antiplatelet agents, as well as targeting platelet transfusions to offer blood products to the patients who need it most. Given that bleeding risk is multifactorial, developing additional assays based on different transduction mechanisms may complement current techniques and offer improved capabilities to detect platelet dysfunction and bleeding risk.

We performed MCATS on $n = 6$ healthy subjects as well as $n = 7$ patients pre- and post-CPB (Fig. 5a). The demographic information and related health information for these subjects can be found in Supplementary Table 3. All patients who had undergone CPB were tested using TEG (using a TEG6S system) and aggregometry in the clinic pre- and post-surgery, and these measurements were benchmarked against MCATS. Note that, due to low count platelet, one subject did not have an accompanying aggregometry measurement. The MCATS score for each donor was averaged from $n = 3$ or 4 replicate measurements where 2×10^6 platelets were seeded in a well and the fluorescence intensity was measured at $t = 1$ h after seeding. In general, healthy donors ($n = 6$) showed similar MCATS tension signal, which was greater than that for CPB donors before surgery, probably because many of the patients undergoing CPB had underlying health conditions, but this premise is yet to be validated. After CPB, subjects showed a significantly reduced MCATS signal (decrease of $35 \pm 11\%$, $P = 0.0002$) that ranged from 48% to 17% (Fig. 5b). Within 24 h after CPB, five out of the seven patients required platelet transfusion to minimize bleeding. We hypothesized that the magnitude of MCATS signal reduction (mechanical dysfunction) is an indicator of the severity of platelet dysfunction, and hence we compared the change in MCATS signal (%) to the number of units of transfused platelets (Fig. 5c). We found that the number of transfused platelets given to the patient in the operating room and within 24 h after surgery was strongly positively correlated with the drop in platelet MCATS signal (Fig. 5c, Pearson's $r = 0.83$, $P = 0.020$). As expected, aggregometry analysis (with 10 μM of ADP) of the same samples showed a decrease of $52 \pm 15\%$, $P = 0.04$ in primary aggregation following CPB. TEG showed a decrease of $25 \pm 5\%$, $P = 0.006$ in maximum aggregation (MA) for the same cohort (Fig. 5d,f). Note that one of the CPB subjects showed an increase in aggregometry value following surgery which further underscores the variability in aggregometry. When the aggregometry and TEG signal change was compared with the number of platelet units transfused, we found a weakly positive correlation for aggregometry and a strong correlation for TEG (Fig. 5e,g, Pearson's $r = 0.48$, $P = 0.33$ for aggregometry and Pearson's $r = 0.84$, $P = 0.018$ for TEG). Our initial pilot study indicates that the mechanical forces generated by platelets offer a unique metric to quantify platelet function. The MCATS assay produces a readout that is correlated with bleeding risk and provides a comparable functional test on par with methods currently used in the operating room such as TEG. Thus, MCATS may offer a complementary indicator of post-operative bleeding risk following CBP.

We also performed controls to validate MCATS measurement for subjects following CPB. Following standard-of-care procedures, patients were treated with heparin before surgery to minimize blood clotting and this was neutralized with protamine post operation. To confirm that the decrease in MCATS signal is not due to inhibition of heparin, we performed MCATS on controlled platelets that were treated with heparin and then neutralized with protamine. The results showed that heparin led to a slight decrease in MCATS signal, but this inhibition was fully reversed upon protamine treatment (Supplementary Fig. 7). We also tested the mechano-IC_{50} of aspirin and ticagrelor for the CPB donors before and after surgery. The results showed that the surgery did not influence the mechano-IC_{50} significantly (Extended Data Fig. 8), which confirms that MCAT is insensitive to platelet count.

Discussion

The current state-of-the-art tools for measuring platelet function are based on aggregometry and viscoelastic assays (TEG)[56], which are routinely used in clinical practice. Aggregometry measures the light transmission of PRP samples using an instrument that applies shear as well as a specific agonist such as ADP and TRAP. Aggregometry records multiple parameters including the kinetics of aggregation to infer clotting functions. Similarly, TEG records the drag forces in whole blood samples, which measures the kinetics of clot formation and viscoelastic properties of clots. The limitations of these assays are multifold. First, unlike MCATS, which requires a standard well plate reader that is already used for most enzyme-linked immunosorbent assays, TEG and aggregometry assays require dedicated instruments. Secondly, LTA and TEG require approximately millilitre quantities of blood for each measurement, which may not seem significant for healthy adults but may be more challenging for patients experiencing thrombocytopenia or bleeding or for neonates. Moreover, creating drug dose–response curves such as those shown in Fig. 4 from a single blood draw would be fairly challenging using LTA and TEG. Even more importantly, TEG and LTA assays have limited sensitivity given that these assays require platelet aggregation, which is highly dependent on platelet count, coagulation factors such as fibrinogen level and antiplatelets agent usage[57–59]. Patients with higher platelet counts will tend to form more stable aggregates regardless of the functional activity of each individual platelet[60], and patients with a low platelet count due to surgery or underlying conditions have difficulty in TEG and aggregometry assays. According to the PLATFORM study, aggregometry shows limited predictive value in identifying post operative bleeding following CPB[52]. Indeed, in our work, we encountered one patient with a low platelet count, which would present a significant challenge for TEG, but this did not hamper

Fig. 5 | MCATS detects platelet dysfunction for patients who had undergone CPB. a, Schematic of workflow using MCATS to assess platelet dysfunction following CPB. Created with BioRender.com. **b**, Plot of MCATS platelet signal for healthy donors ($n = 6$), pre-CPB and post-CPB subjects ($n = 7$). Error bars represent s.d. from $n = 4$ measurements for the same platelet sample. Significance is calculated with two-tailed t-test with $P = 0.0002$. *** represents a P value <0.001. **c**, Plot of MCAT reduction in signal (%) against the number of platelets transfusions given to the subject within 24 h of CPB. Data points are colour coded for each subject and represent the mean percentage loss of mechanical force in the patient platelets before and after surgery. Error bars represent s.d. of $n = 3$ measurements, and centre represents mean of three measurements. Pearson's correlation coefficient $r = 0.83$ with two-tailed $P = 0.020$. **d**, Plot of aggregometry PA (mm) for subjects pre-CPB and post-CPB. **e**, Plot of aggregometry PA decrease (%) versus platelet transfusion needs within 24 h of CPB. Note that one patient lacked aggregometry data because of severe haemolysis. Pearson's correlation coefficient $r = 0.48$ with two-tailed $P = 0.33$. **f**, Plot of TEG MA (mm) for subjects pre-CPB and post-CPB. **g**, Plot of TEG MA decrease (%) versus platelet transfusion need. Pearson's correlation coefficient $r = 0.84$ with two-tailed $P = 0.018$.

https://doi.org/10.1038/s41551-023-01114-1

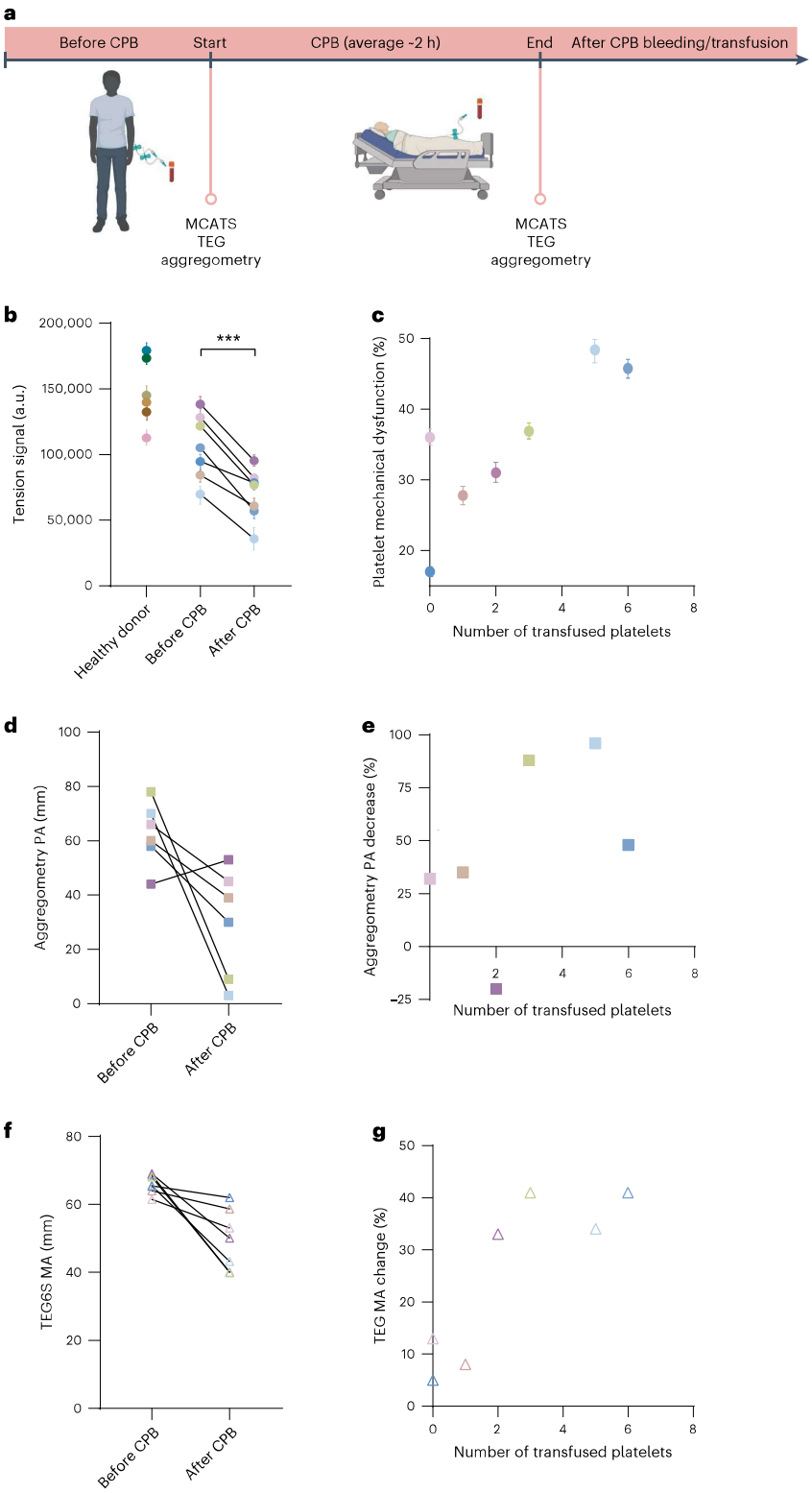

the MCATS assay. Considering that platelet count is closely linked with coagulation, we analysed the relationship between platelet count and the clinical platelet transfusion need. When we plotted platelet count against the number of transfused platelet units we found a positive correlation that was not statistically significant ($r = 0.72$, $P = 0.07$; Supplementary Fig. 8). This is consistent with the literature as platelet count is only one factor in determining bleeding risk. In patients undergoing chemotherapy, for example, platelet count by itself does not determine bleeding risk[61]. Thus, MCATS offer an orthogonal and complementary measurement of platelet function with potential clinically relevance. We envision that MCATS will complement LTA and TEG, both of which are highly platelet count dependent[62,63].

We found that the decreased platelet tension in patients who had undergone CPB is correlated with need for platelet transfusion to minimize bleeding. Further underscoring the importance of platelet force in bleeding, it is demonstrated in the literature that peak platelet force after CPB was significantly lower, which is likely to play a role in CPB-associated microvascular haemorrhage[64]. However, the process of coagulation involves a complex cascade and diverse factors in CPB contribute to coagulopathy. The factors include physical factors (shear flow and hypothermia), exposure to artificial material, drug administration and the release of endogenous chemicals. Due to this complexity, the mechanism behind the observed correlation between bleeding and mechanical forces in CPB remains unclear.

During complicated cardiovascular surgery, CPB is used to maintain blood flow and oxygen delivery while diverting blood away from surgical site. It has been reported that this process will lead to platelet activation and a change of cell shape as well as membrane protein presentation[65]. Importantly, it is reported that GPIb level decreased significantly after surgery[50]. Additionally, research has shown that GPIIb/IIIa drops significantly soon after CPB and is maintained at low levels 2–4 h after the surgery[66,67]. The decrease in receptor expression may root from plasmin generated during CPB, which cleaves GPIIb/IIIa (ref. 68). The acute activation of platelet may also lead to platelet exhaustion, which can lead to a defective platelet aggregation[69]. Another potential mechanism for platelet dysfunction and decreased platelet contractility involves the activation of von Willebrand factor (VWF) during CPB. In disease models such as acquired von-Willebrand syndrome, it has been shown that platelet GPIIb/IIIa is inhibited following changes in VWF[70,71]. The change in GPIb and GPIIb/IIIa is probably a main factor in altered mechanical force generation of platelets as they are the main mechanosensing and mechanotransduction hub of platelets. During haemostasis, platelets will interact with adhesive ligands such as VWF through GPIb, anchoring the platelets to the injured site[72]. Then, platelet aggregation is facilitated by the binding of surface integrin $\alpha_{IIb}\beta_3$ to fibrin and fibrinogen, collagen and fibronectin[73]. The contractility of the receptors to their surroundings contribute to the strength of the platelet plug and may help re-approximate damaged vascular endothelium[74].

Current gold-standard diagnostic methods for potential bleeding such as TEG measure the viscoelastic properties of clots, which is fundamentally linked to platelet force and the contraction against each other. Other methods that use micropatterned polymer structures to measure the platelet traction force have been used to demonstrate that platelet traction force is correlated to bleeding such as trauma-induced coagulopathy[17], genetic bleeding disorder such as May Hegglin disorder and Wiskott Aldrich syndrome[16], and immune thrombocytopenia purpura[75]. These studies further validate the importance of measuring force in different bleeding pathological settings.

One potential clinical use of MCATS may be in predicting severe bleeding. The universal definition for perioperative bleeding in adult cardiac surgery stratifies patients into five classes, where classes 1 and 2 are defined as insignificant, and mild bleeding, while classes 3, 4 and 5 indicate moderate, severe and massive bleeding, respectively[48]. The definition is based on a number of factors including blood loss and allogeneic blood product transfusion. We followed this definition and classified patients who had undergone CPB on the basis of clinical observations. We found that patients with moderate, severe or massive bleeding (classes 3, 4 or 5) showed a more significant drop in MCATS score compared with patients with mild or insignificant bleeding (Extended Data Fig. 9). Because MCATS exclusively quantifies platelet function, more studies are needed for understanding the correlation between platelet function and bleeding risk.

Another unique merit of MCATS is that it measures the aggregate number of mechanical events with $F > T_{tol}$ directly using a conventional plate reader. As a result, MCATS only requires ~5 µl of blood or less, and hence a typical blood draw (~5 ml) is enough to run 1,000 assays. Antiplatelet therapies are commonly prescribed to prevent acute arterial thrombosis. However, antiplatelet therapy assessment based on aggregometry has not shown improved outcomes and better benefit/risk for the patient[76]. MCATS can generate personalized dose–response curves for specific drugs rapidly to optimize treatment in a dynamic manner, which may increase the sensitivity and specificity required to guide personalized platelet therapy. So far, we measured the forces applied by GPIIb/IIIa, which mediates platelet adhesion and aggregation to assess platelet functions. Other platelet forces mediated by GPIb-IX-V and GPVI can potentially be investigated by attaching different ligands/proteins on DNA tension probe to understand the platelet forces with different receptors under shear flow or in different haemostasis states[77]. It is also worth noting that live and active cells are required to perform MCATS, and we confirmed that lyophilized platelets (fixed platelets with intact protein structure) failed to generate MCATS signal (Extended Data Fig. 10).

In MCATS experiments, different platelet handling procedures may alter platelet response. Therefore, we tested different platelet purification procedures, and the results indicated that MCATS can detect tension signal from purified platelets, PRP and whole blood samples. However, whole blood showed decreased tension signal in MCATS because the high abundance of red blood cells blocked access to the chip surface. We anticipate that applying mild flow conditions would better allow performing MCATS in whole blood. PRP showed slightly decreased MCATS signal compared with that when using purified platelets. Advantages of using PRP include simplifying blood processing steps and decreasing preparation time to run the assay (Supplementary Fig. 5). Other advantages of using PRP include maintaining the physiological drug dose found in the blood, which is important for assessing drugs that have short half-life or rapid off-rates. Conversely, the use of purified platelets for MCATS enhanced the signal and provided a more direct evaluation of platelet function without interference from soluble factors. However, MCATS measures the mechanical rupture event from cellular receptors under static conditions, while platelets function under conditions of shear flow. Thus, MCATS may not fully capture the mechanical response of platelets in vivo. Further optimization of the device under flow may be required for more accurate measurement of platelet response in more physiological conditions. Because the assay is performed on glass surfaces, this exposed platelets to substrates with considerably large stiffness that probably perturbs inherent responses. Additionally, we adopted cRGD in current design for engagement with GPIIb/IIIa, which primarily reports on mechanical force transmission from GPIIb/IIIa. MCATS probes that present VWF may lead more comprehensive analysis of platelet force generation. Additionally, other parameters such as coagulation factors such as fibrinogen, VWF and others as well as platelet count all influence the coagulation cascade. Hence, combining the results of conventional assays (TEG and LTA) that are already used in the clinic with MCATS may help improve characterization of bleeding risk.

Another important parameter to consider in MCATS is the assay time. We monitored MCATS signal in platelet and fibroblast experiments with different amplification times. The results showed that 30 min amplification provides sufficient signal, but signal could be

further enhanced at 60 min. Further increasing amplification time did not lead to significantly improved S/N (Supplementary Fig. 9). These results indicate that MCATS has potential as a point-of-care assay given the 30 min or 60 min response time.

Because MCATS measures the accumulated number of mechanical events generated by specific receptors, investigating different cell types or different types of receptors requires optimization of the tension sensor to maximize S/N. For example, we tested both 12-pN and 56-pN probes for human platelets and fibroblasts, and it was shown that 12-pN probes generated greater MCATS signal in these two cell types. Other cell types such as smooth muscle cells and keratinocytes have been reported to generate significantly greater traction forces, and hence greater T_{tol} probes would be appropriate for such models[8,78]. The force threshold should be chosen carefully for different applications.

MCATS provides a sensitive and rapid assay that reports on the total number of molecular force events using a conventional plate reader. The assay may provide a useful tool for the scientific community to study mechanobiology broadly. We envision areas that include the screening of how different adhesion ligands, drugs and genes as well as cell state and metabolites can modulate traction forces in a high-throughput manner.

Methods

Materials

Cy3B–NHS ester (PA63101) was purchased from GE Healthcare Life Sciences. Atto647N–NHS ester (18373) was purchased from Sigma-Aldrich. Cyclo[Arg–Gly–Asp–D-Phe–Lys(PEG–PEG)] (PCI-3696-PI) (cRGD) was acquired from Peptides International. Streptavidin (S000-01) was purchased from Rockland-Inc. μ-Slide VI0.4 6-channel slides (80606) and 25 mm × 75 mm glass coverslips (10812) were purchased from Ibidi. ProPlate Microtiter (204969) was purchased from Grace Bio-Labs. 200 proof ethanol (100%, #04-355-223) was purchased from Fischer Scientific. *N*-Hydroxyl succinimide-5 kDa PEG–biotin (NHS–PEG–biotin, HE041024-5K) was purchased from Biochempeg. 3-Aminopropyl triethoxysilane (440140, 99% purity) and ADP (A2754, 95% purity) were purchased from Sigma-Aldrich. Tris-hydroxypropyltriazolylmethylamine was purchased from Click Chemistry Tools. Ticagrelor was acquired from Selleck Chemistry. 7E3 (Abciximab, Lot: GR3422387-2) was purchased from Abcam and diluted to a series of concentration when used. Anti-integrin $\alpha_V\beta_3$ antibody (clone LM609, MAB1976, Lot: 3863390) and anti-integrin $\alpha_5\beta_1$ antibody (clone JBS5, MAB1969-I, Lot#3941858) were purchased from Sigma-Aldrich and used at 1:100 dilution and 1:50 dilution, respectively. Apyrase and LbCas12 were purchased from New England Biolabs. All DNA oligonucleotides used in this work are listed in Supplementary Table 1 and were custom synthesized by Integrated DNA Technologies. CRISPR RNA was custom synthesized by Dharmacon. All other reagents and materials (unless otherwise stated) were purchased from Sigma-Aldrich and used without purification. All buffers were prepared with 18.2 MΩ nanopure water.

Instruments

We used a Nikon Eclipse Ti microscope, operated by Nikon Elements software, and equipped with a 1.49 numerical aperture (NA) CFI Apo ×100 objective, perfect focus system, a total internal reflection fluorescence (TIRF) laser launch, a Chroma quad cube (ET-405/488/561/640 nm Laser Quad Band) and a reflection interference contrast microscope (RICM; Nikon: 97270) cube for this work. Bulk fluorescence measurements were conducted using a Synergy H1 plate reader (Bio-Tek) using fluorescence filter sets. All ultrapure water was obtained from a Barnstead Nanopure water purifying system (Thermo Fisher) that indicated a resistivity of 18.2 MΩ. Nucleic acid purification was performed using high-performance liquid chromatography (HPLC, Agilent 1100) equipped with a diode array detector. Microvolume absorbance measurements were obtained using a Nanodrop 2000 UV–Vis Spectrophotometer (Thermo Scientific). Vacufuge Plus (Eppendorf) was used to remove solvent from HPLC-purified sample. ESI mass spectrometry identification of product was performed with an Exactive Plus Orbitrap Mass Spectrometer. MJ Research PTC-200 Thermal Cycler was used to anneal and hybridize DNA. Platelet counts were determined on a Poch-100i hematology analyzer.

Surface preparation

MCATS surface preparation was adapted from previously published protocols[20,79]. Briefly, rectangular glass coverslips (25 × 75 mm, Ibidi) were rinsed with water and sonicated for 20 min in de-ionized water, and then this was repeated for another 20 min in ethanol. The glass converslips were then cleaned with piranha solution, which was prepared using a 1:3 mixture of 30% H_2O_2 and H_2SO_4 (ref. 80). Warning: piranha solution becomes very hot upon mixing, and is highly oxidizing and may explode upon contact with organic solvents. Please handle with care. Slides were then washed six times in ultrapure water, followed by four successive washes using ethanol. In a separate beaker of ethanol, slides were reacted with 3% v/v 3-aminopropyl triethoxysilane at room temperature for 1 h. Coverslips were then washed six times with ethanol, baked in an oven for 20 min at 80 °C. Subsequently, the amine terminal groups were coupled to 5 kDa NHS–PEG–biotin (3% w/v) by placing 200 μl of a freshly prepared 6 mM NHS–PEG–biotin solution in ultrapure water between two slides for 1 h. Next, slides were washed three times with ultrapure water, dried under N_2 gas and then stored at −30 °C for up to 2 weeks or longer before use. At the day of imaging, the 5 kDa PEG–biotin substrate was adhered to a ProPlate microtitre 96-well plate housing with an adhesive bottom. Wells were then incubated with 50 μg ml^{-1} (830 nM) streptavidin in 1× phosphate-buffered saline (PBS) for 1 h. Wells were then washed with 1× PBS and incubated with 100 nM DNA probe solutions for 1 h. Finally, the wells were washed with 1× PBS.

DNA hybridization and gRNA–Cas12a binding

DNA oligonucleotides were hybridized at 100 nM in a 0.2-ml PCR tube before incubating on the surface. Using an MJ Research PTC-200 thermocycler, DNA was first heated to 90 °C and then cooled at a rate of 1.3 °C min^{-1} to 35 °C. gRNA and Cas12a were incubated for 10 min at 37 °C at 500 nM in a 0.2-ml PCR tube just before adding to the surface and stored on ice for maximum preservation of activity.

Oligo dye and ligand coupling and purification

All sequences of DNA strands used in this work are provided in Supplementary Table 1. To generate the dye-labelled bottom strand, 10 nmol of amine-modified DNA was reacted overnight at 4 °C with a 20× excess of Cy3B–NHS or ATTO 647N–NHS dissolved in 10 μl dimethyl sulfoxide. The total volume of the reaction was 100 μl, and this was composed of 1× PBS supplemented with 0.1 M $NaHCO_3$. Then a P2 size exclusion gel was used to remove unreacted dye. The product **1** or **2** (Supplementary Fig. 3) was then purified by reverse-phase HPLC using an Agilent Advanced oligo column (solvent A: 0.1 M triethylammonium acetate, solvent B: acetonitrile; starting condition: 90% A + 10% B, 1% min^{-1} gradient B, flow rate 0.5 ml min^{-1}) (Supplementary Fig. 3).

To generate the cRGD-modified top strand (product **3** in Supplementary Fig. 3), 100 nmol of c(RGDfK (PEG–PEG)) was reacted with ~200 nmol of NHS–azide in 15 μl of dimethyl sulfoxide overnight at 4 °C. Product **3** was then purified via reverse-phase HPLC using a Grace Alltech C18 column (solvent A: water + 0.05% trifluoroacetic acid, solvent B: acetonitrile + 0.05% trifluoroacetic acid; starting condition: 90% A + 10% B, 1% min^{-1}; flow rate: 1 ml min^{-1}).

Purified product **3** was ligated to the BHQ2 top strand via 1,3-dipolar cycloaddition click reaction. Briefly, 5 nmol of alkyne-modified top strand was reacted with ~70 nmol of product **3**. The total reaction volume was 50 μl, composed of 0.1 M sodium ascorbate and 0.1 mM Cu-Tris-hydroxypropyltriazolylmethylamine for 2 h at room temperature. Product **4** was then purified with a P2 size exclusion column, and then purified with reverse phase HPLC using an Agilent Advanced

oligo column (solvent A: 0.1 M triethylammonium acetate, solvent B: acetonitrile; starting condition: 90% A + 10% B, 0.5% min^{-1} gradient B, flow rate: 0.5 ml min^{-1}) (Supplementary Fig. 3).

Concentrations of purified oligonucleotide conjugates were determined by measuring their absorption at l = 260 nm on a Nanodrop 2000 UV–Vis spectrophotometer (Thermo Scientific). ESI–mass spectrometry was performed to validate all oligonucleotide products, and the results are listed in Supplementary Table 2.

Solution based Cas12a amplification and plate reader readout

Cas12a reactions reported in Fig. 1e were performed at 37 °C for 1 h in 1× PBS supplemented with 10 mM $MgCl_2$. For these measurements, we maintained a total DNA (60 T bottom strand, Supplementary Table 1) solution concentration of 100 nM but tuned the ratio between the blocked DNA and unblocked activator. We prepared freshly primed Cas12a by mixing with gRNA at 1:1 ratio. The primed Cas12a–gRNA complex was then mixed at 20 nM concentration with 100 nM fluorogenic reporter to the well. Then we measured the final fluorescence intensity using a plate reader using a filter set (Ex/Em = 540/590 nm for reporter channel) after allowing the reaction to proceed for 1 h.

Human platelet handling and ethics agreement

Blood was collected at Emory Hospital from consented patients/volunteers. For patients, blood was collected from arterial line into 5-ml 3.2% citrate tubes (9:1 v/v) at baseline and after CPB (after protamine treatment). For healthy volunteers, blood was collected by venipuncture into citrate tubes as above. Complete blood count was performed using Poch-100i hematology analyzer (Sysmex Corp) to evaluate platelet count. The sample was then centrifuged for 12 min at 140g (with 0.02 U apyrase). Then PRP was separated and centrifuged for 5 min at 700g with 3 µM PGE-1. The platelets were then resuspended in Tyrodes buffer with 3 µM PGE-1 and centrifuged for 5 min at 700g. Finally, platelets were resuspended in Tyrodes buffer. It is worth noting that apyrase is important for the platelet purification procedure to prevent haemolysis-triggered platelet aggregation.

This project has approval from the Emory University Ethics Committee to obtain samples from participants, and these ethical regulations cover the work in this study. Written informed consent was obtained from all participants.

Cell culture

NIH/3T3 fibroblasts and HeLa cells were cultured according to ATCC guidelines. Briefly, cells were cultured in Dulbecco's modified Eagle medium (DMEM) supplemented with 10% bovine calf serum (v/v, purchased from Gibco) and penicillin–streptomycin. Cells were passaged every 2–3 days as required.

MCATS

MCATS was performed on activated substrates as described in the surface preparation section. First, cRGDfK-labelled concealed activator probes were incubated on biotin surfaces in 1× PBS buffer for 1 h. The wells were washed with 1× PBS. Then, cells were added and allowed to spread on the surfaces for 1 h in specific media (DMEM supplemented with 1% serum for NIH/3T3 cells and Tyrodes buffer with 10 µM ADP for platelets). Surfaces were imaged at approximately 1 h after seeding using epifluorescence and TIRF microscopy to visualize and quantify mechanically exposed activators. Wells were then supplemented with 10 mM $MgCl_2$, and subsequently, 20 nM gRNA/Cas12a complex and 100 nM reporter DNA were mixed and added to the well to initiate the Cas12a amplification reaction with mechanically exposed activator. After 1 h of triggering the Cas12a reaction, fluorescence intensities of wells were measured with a Bio-Tek Synergy H1 plate reader (Ex/Em = 540/590 nm for reporter channel). Note that we always included positive and negative control wells to help benchmark the MCATS signal. The positive control wells were composed of 100% surface-tethered activator oligonucleotides, while the negative control was the blocked activator.

Dose-dependent inhibition of receptor-mediated tension

For dose-dependent inhibition of fibroblast experiments, the cell density of 3T3 fibroblast was first characterized with a haemocytometer. A total of 25×10^3 cells were incubated with different concentrations of inhibitor in the cell culture incubator for 30 min before plating onto 96-well plates. Afterwards, cells were incubated for 1 h to promote cell adhesion. Then the MCATS protocol was followed to achieve amplification and quantification.

For platelet MCATS measurements, human platelets were purified and stored at room temperature for at least 30 min before running experiments. For the drug treatment measurements, platelets were treated with each drug for 30 min before seeding onto 96-well plates. Then 10 µM ADP was added to the well to promote cell activation and adhesion, and platelets were incubated at room temperature for 1 h. The same MCATS protocols that were used for fibroblasts were also followed to achieve amplification and quantification of force generation by platelets.

For HeLa cell integrin subtype inhibition experiments, the cell density of Hela cells was first characterized with a haemocytometer. A total of 20×10^3 cells were incubated with 10 µg ml^{-1} monoclonal antibody of integrin $\alpha_5\beta_1$ (1:100 dilution) or $\alpha_V\beta_3$ (1: 50 dilution) for 30 min before running MCATS assays.

Microscopy imaging

For MCATS experiments, images were acquired on a Nikon Eclipse Ti microscope, operated by Nikon Elements software, a 1.49 NA CFI Apo 100× objective, perfect focus system and a TIRF laser launch with 488 nm (10 mW), 561 nm (50 mW) and 638 nm (20 mW). An RICM (Nikon: 97270) cube and a Chroma quad cube (ET-405/488/561/640 nm Laser Quad Band) were used for imaging. Images were analysed using ImageJ. Imaging was performed on 96-well plates and glass coverslips using DMEM as cell imaging medium for 3T3 cells and Tyrode's buffer for platelets. All imaging data were acquired at room temperature.

TEG

TEG measurements were obtained in the operating room using the TEG 6S system (Haemonetics) according to manufacturer instructions. This is a fully automated point-of-care system shown to have excellent agreement with the TEG 5000 (Haemonetics), which has been widely used in cardiac surgery for purposes of guiding haemostatic blood product transfusions[81]. Briefly, 2.7 ml of whole blood was collected from the subject's pre-existing arterial line into 3.2% citrated tubes. Following the recommended wait time of 10 min, approximately 400 µl of whole blood was pipetted into the sample port of a global haemostasis cartridge (Haemonetics). The parameter of interest was the maximum amplitude (MA) of the standard kaolin activated channel. The MA reflects the strength of platelet–fibrinogen interactions.

Light transmission platelet aggregometry

To isolate PRP, blood collected from volunteers/patients was centrifuged at room temperature at 100g for 12 min in Megafuge 16R (ThermoScientific) equipped with swinging bucket rotor. The PRP layer was removed, and platelet count was obtained and, if necessary, adjusted to less than 400,000 $µl^{-1}$. Next, samples were re-centrifuged at 2,000g for 20 min to obtain platelet-poor plasma. LTA was accomplished using PAP-8E profiler (Biodata Corp.) pre-warmed to 37 °C. The blank (0% aggregation) was set with platelet-poor plasma. For the testing, ADP and TRAP-6 were used as platelet activators. The final concentrations used were 20 and 10 µM for ADP and 10 µM for TRAP. All LTA testing was performed according to manufacturer's directions. Percentage aggregation (PA), slope, area under the curve, lag phase, disaggregation, MA and final aggregation were recorded.

Statistics and reproducibility

P values were determined by two-tailed Student's *t*-test using GraphPad Prism8. Correlation analysis is conducted using GraphPad Prism8 to acquire Person's *r* in Fig. 4. Mechano-IC_{50} is calculated by fitting plot to a standard dose–response function: Signal = Bottom + (Top − Bottom)/(1 + ([drug]/IC_{50})) using GraphPad Prism8. Each MCATS readout is typically replicated with two to four wells on the same plate for the same condition. For the tension signal of patients who had undergone CPB, all data were acquired along with positive and negative control wells to help benchmark signal. The positive control wells were composed of 100% surface-tethered activator oligonucleotides, while the negative control was the blocked activator without platelet seeding. MCATS signal for each run was normalized to the positive control wells also conducted in each experiment and then multiplied by the average intensity of the positive wells collected from past positive control runs. This normalization process helped to minimize the influence of variance in enzyme activity (batch-to-batch variability) along with variability in the surfaces and other sources of experimental noise.

Reporting summary

Further information on research design is available in the Nature Portfolio Reporting Summary linked to this article.

Data availability

The data supporting the results in this study are available within the paper and its Supplementary Information. Raw data and images were deposited in Dataverse and can be accessed via the identifier https://doi.org/10.15139/S3/4Q8H1A. All raw and analysed datasets are available from the corresponding authors on request. No identifiable information from the participants will be disclosed. Source data are provided with this paper.

References

1. Orr, A. W., Helmke, B. P., Blackman, B. R. & Schwartz, M. A. Mechanisms of mechanotransduction. *Dev. Cell* **10**, 11–20 (2006).
2. Zhang, Y. et al. Platelet integrins exhibit anisotropic mechanosensing and harness piconewton forces to mediate platelet aggregation. *Proc. Natl Acad. Sci. USA* **115**, 325–330 (2018).
3. Ma, R. et al. DNA probes that store mechanical information reveal transient piconewton forces applied by T cells. *Proc. Natl Acad. Sci. USA* **116**, 16949–16954 (2019).
4. Ramey-Ward, A. N., Su, H. & Salaita, K. Mechanical stimulation of adhesion receptors using light-responsive nanoparticle actuators enhances myogenesis. *ACS Appl. Mater. Interfaces* **12**, 35903–35917 (2020).
5. Wang, X. & Ha, T. Defining single molecular forces required to activate integrin and notch signaling. *Science* **340**, 991–994 (2013).
6. Gaudet, C. et al. Influence of type I collagen surface density on fibroblast spreading, motility, and contractility. *Biophys. J.* **85**, 3329–3335 (2003).
7. Zhang, Y., Ge, C., Zhu, C. & Salaita, K. DNA-based digital tension probes reveal integrin forces during early cell adhesion. *Nat. Commun.* **5**, 5167 (2014).
8. Rashid, S. A. et al. DNA tension probes show that cardiomyocyte maturation is sensitive to the piconewton traction forces transmitted by integrins. *ACS Nano* **16**, 5335–5348 (2022).
9. Su, H. et al. Massively parallelized molecular force manipulation with on-demand thermal and optical control. *JACS* **143**, 19466–19473 (2021).
10. Doudna, J. A. & Charpentier, E. The new frontier of genome engineering with CRISPR–Cas9. *Science* **346**, 1258096 (2014).
11. Kaminski, M. M., Abudayyeh, O. O., Gootenberg, J. S., Zhang, F. & Collins, J. J. CRISPR-based diagnostics. *Nat. Biomed. Eng.* **5**, 643–656 (2021).
12. Chen, J. S. et al. CRISPR–Cas12a target binding unleashes indiscriminate single-stranded DNase activity. *Science* **360**, 436–439 (2018).
13. Gootenberg, J. S. et al. Multiplexed and portable nucleic acid detection platform with Cas13, Cas12a, and Csm6. *Science* **360**, 439–444 (2018).
14. Broughton, J. P. et al. CRISPR–Cas12-based detection of SARS-CoV-2. *Nat. Biotechnol.* **38**, 870–874 (2020).
15. Xiong, Y. et al. Functional DNA regulated CRISPR–Cas12a sensors for point-of-care diagnostics of non-nucleic-acid targets. *J. Am. Chem. Soc.* **142**, 207–213 (2019).
16. Myers, D. R. et al. Single-platelet nanomechanics measured by high-throughput cytometry. *Nat. Mater.* **16**, 230–235 (2017).
17. Ting, L. H. et al. Contractile forces in platelet aggregates under microfluidic shear gradients reflect platelet inhibition and bleeding risk. *Nat. Commun.* **10**, 1204 (2019).
18. Cuisset, T. et al. Relationship between aspirin and clopidogrel responses in acute coronary syndrome and clinical predictors of non response. *Thromb. Res.* **123**, 597–603 (2009).
19. Neira, H. D. & Herr, A. E. Kinetic analysis of enzymes immobilized in porous film arrays. *Anal. Chem.* **89**, 10311–10320 (2017).
20. Duan, Y. et al. Mechanically triggered hybridization chain reaction. *Angew. Chem. Int. Ed.* **60**, 19974–19981 (2021).
21. Glazier, R. et al. DNA mechanotechnology reveals that integrin receptors apply pN forces in podosomes on fluid substrates. *Nat. Commun.* **10**, 4507 (2019).
22. Wang, X. et al. Integrin molecular tension within motile focal adhesions. *Biophys. J.* **109**, 2259–2267 (2015).
23. Sahai, E., Ishizaki, T., Narumiya, S. & Treisman, R. Transformation mediated by RhoA requires activity of ROCK kinases. *Curr. Biol.* **9**, 136–145 (1999).
24. Oba, M. et al. Cyclic RGD peptide-conjugated polyplex micelles as a targetable gene delivery system directed to cells possessing αvβ3 and αvβ5 integrins. *Bioconjug. Chem.* **18**, 1415–1423 (2007).
25. Riikonen, T., Vihinen, P., Potila, M., Rettig, W. & Heino, J. Antibody against human α1β1 integrin inhibits HeLa cell adhesion to laminin and to type I, IV, and V collagens. *Biochem. Biophys. Res. Commun.* **209**, 205–212 (1995).
26. Yamada, Y. et al. Structure-activity relationships of RGD-containing peptides in integrin αvβ5-mediated cell adhesion. *ACS Omega* **8**, 4687–4693 (2023).
27. Belkin, A. M. et al. Transglutaminase-mediated oligomerization of the fibrin(ogen) αC domains promotes integrin-dependent cell adhesion and signaling. *Blood* **105**, 3561–3568 (2005).
28. Roca-Cusachs, P., Gauthier, N. C., Del Rio, A. & Sheetz, M. P. Clustering of α5β1 integrins determines adhesion strength whereas αvβ3 and talin enable mechanotransduction. *Proc. Natl Acad. Sci. USA* **106**, 16245–16250 (2009).
29. Galior, K., Liu, Y., Yehl, K., Vivek, S. & Salaita, K. Titin-based nanoparticle tension sensors map high-magnitude integrin forces within focal adhesions. *Nano Lett.* **16**, 341–348 (2016).
30. Brockman, J. M. et al. Live-cell super-resolved PAINT imaging of piconewton cellular traction forces. *Nat. Methods* **17**, 1018–1024 (2020).
31. Brockman, J. M. et al. Mapping the 3D orientation of piconewton integrin traction forces. *Nat. Methods* **15**, 115–118 (2018).
32. Hu, Y. et al. DNA-based microparticle tension sensors (μTS) for measuring cell mechanics in non-planar geometries and for high-throughput quantification. *Angew. Chem. Int. Ed.* **133**, 18192–18198 (2021).
33. Dias, J. D. et al. Comparison of three common whole blood platelet function tests for in vitro P2Y12 induced platelet inhibition. *J. Thromb. Thrombolysis* **50**, 135–143 (2020).
34. Le Blanc, J., Mullier, F., Vayne, C. & Lordkipanidzé, M. Advances in platelet function testing—light transmission aggregometry and beyond. *J. Clin. Med.* **9**, 2636 (2020).

35. Davidson, B. L. et al. Bleeding risk of patients with acute venous thromboembolism taking nonsteroidal anti-inflammatory drugs or aspirin. *JAMA Intern. Med.* **174**, 947–953 (2014).
36. Awtry, E. H. & Loscalzo, J. Aspirin. *Circulation* **101**, 1206–1218 (2000).
37. Phillips, D. R. & Scarborough, R. M. Clinical pharmacology of eptifibatide. *Am. J. Cardiol.* **80**, 11B–20B (1997).
38. Tcheng, J. E. et al. Pharmacodynamics of chimeric glycoprotein IIb/IIIa integrin antiplatelet antibody Fab 7E3 in high-risk coronary angioplasty. *Circulation* **90**, 1757–1764 (1994).
39. Roth, G. & Majerus, P. W. The mechanism of the effect of aspirin on human platelets. I. Acetylation of a particulate fraction protein. *J. Clin.* **56**, 624–632 (1975).
40. Tardiff, B. E. et al. Pharmacodynamics and pharmacokinetics of eptifibatide in patients with acute coronary syndromes. *Circulation* **104**, 399–405 (2001).
41. Sassoli, P. M. et al. 7E3 F (ab') 2, an effective antagonist of rat αIIbβ3 and αvβ3, blocks in vivo thrombus formation and in vitro angiogenesis. *Thromb. Haemost.* **85**, 896–902 (2001).
42. Aungraheeta, R. et al. Inverse agonism at the P2Y12 receptor and ENT1 transporter blockade contribute to platelet inhibition by ticagrelor. *Blood* **128**, 2717–2728 (2016).
43. Wang, X. et al. Comparative analysis of various platelet glycoprotein IIb/IIIa antagonists on shear-induced platelet activation and adhesion. *J. Pharmacol. Exp. Ther.* **303**, 1114–1120 (2002).
44. Harder, S. et al. In vitro dose response to different GPIIb/IIIa-antagonists: inter-laboratory comparison of various platelet function tests. *Thromb. Res.* **102**, 39–48 (2001).
45. De La Cruz, J., Bellido, I., Camara, S., Martos, F. & De La Cuesta, F. S. Effects of acetylsalicylic acid on platelet aggregation in male and female whole blood: an in vitro study. *Scand. J. Haemotol.* **36**, 394–397 (1986).
46. Kirkby, N. et al. Antiplatelet effects of aspirin vary with level of P2Y (12) receptor blockade supplied by either ticagrelor or prasugrel. *J. Thromb. Haemost.* **9**, 2103–2105 (2011).
47. Greiff, G. et al. Prediction of bleeding after cardiac surgery: comparison of model performances: a prospective observational study. *J. Cardiothorac. Vasc. Anesth.* **29**, 311–319 (2015).
48. Dyke, C. et al. Universal definition of perioperative bleeding in adult cardiac surgery. *J. Thorac. Cardiovasc. Surg.* **147**, 1458–1463 (2014).
49. Bartoszko, J. et al. Comparison of two major perioperative bleeding scores for cardiac surgery trials: universal definition of perioperative bleeding in cardiac surgery and european coronary artery bypass grafting bleeding severity grade. *Anesthesiology* **129**, 1092–1100 (2018).
50. Kondo, C. et al. Platelet dysfunction during cardiopulmonary bypass surgery. With special reference to platelet membrane glycoproteins. *ASAIO J.* **39**, M550–M553 (1993).
51. Roka-Moiia, Y. et al. Platelet dysfunction during mechanical circulatory support. *Arterioscler. Thromb. Vasc. Biol.* **41**, 1319–1336 (2021).
52. Ranucci, M. et al. Platelet function after cardiac surgery and its association with severe postoperative bleeding: the PLATFORM study. *Platelets* **30**, 908–914 (2019).
53. Welsh, K. J., Padilla, A., Dasgupta, A., Nguyen, A. N. D. & Wahed, A. Thromboelastography is a suboptimal test for determination of the underlying cause of bleeding associated with cardiopulmonary bypass and may not predict a hypercoagulable state. *Am. J. Pathol.* **142**, 492–497 (2014).
54. Welsby, I. J. et al. The kaolin-activated thrombelastograph predicts bleeding after cardiac surgery. *J. Cardiothorac. Vasc. Anesth.* **20**, 531–535 (2006).
55. Bowbrick, V. A., Mikhailidis, D. P. & Stansby, G. Influence of platelet count and activity on thromboelastography parameters. *Platelets* **14**, 219–224 (2003).
56. Choi, J.-L., Li, S. & Han, J.-Y. Platelet function tests: a review of progresses in clinical application. *BioMed. Res. Int.* **2014**, 456569 (2014).
57. Kaufmann, C. R., Dwyer, K. M., Crews, J. D., Dols, S. J. & Trask, A. L. Usefulness of thrombelastography in assessment of trauma patient coagulation. *J. Trauma.* **42**, 716–720 (1997).
58. Moenen, F. C. et al. Screening for platelet function disorders with Multiplate and platelet function analyzer. *Platelets* **30**, 81–87 (2019).
59. Quarterman, C., Shaw, M., Johnson, I. & Agarwal, S. Intra- and inter-centre standardisation of thromboelastography (TEG®). *Anaesthesia* **69**, 883–890 (2014).
60. Harr, J. N. et al. Functional fibrinogen assay indicates that fibrinogen is critical in correcting abnormal clot strength following trauma. *Shock* **39**, 45–49 (2013).
61. Slichter, S. J. et al. Dose of prophylactic platelet transfusions and prevention of hemorrhage. *N. Engl. J. Med.* **362**, 600–613 (2010).
62. Femia, E. A., Scavone, M., Lecchi, A. & Cattaneo, M. Effect of platelet count on platelet aggregation measured by impedance aggregometry (Multiplate™ analyser) and by light transmission aggregometry. *J. Thromb. Haemost.* **11**, 2193–2196 (2013).
63. Boknäs, N., Macwan, A. S., Södergren, A. L. & Ramström, S. Platelet function testing at low platelet counts: when can you trust your analysis? *Res. Pract. Thromb. Haemost.* **3**, 285–290 (2019).
64. Greilich, P. E., Carr, M. E. Jr., Carr, S. L. & Chang, A. S. Reductions in platelet force development by cardiopulmonary bypass are associated with hemorrhage. *Anesth. Analg.* **80**, 459–465 (1995).
65. Zwifelhofer, N. M. J. et al. Platelet function changes during neonatal cardiopulmonary bypass surgery: mechanistic basis and lack of correlation with excessive bleeding. *Thromb. Haemost.* **120**, 94–106 (2020).
66. Holada, K., Šimák, J., Kučera, V., Rožňová, L. & Eckschlager, T. Platelet membrane receptors during short cardiopulmonary bypass—a flow cytometric study. *Perfusion* **11**, 401–406 (1996).
67. Rinder, C. S. et al. Modulation of platelet surface adhesion receptors during cardiopulmonary bypass. *Anesthesiology* **75**, 563–570 (1991).
68. Gouin, I. et al. In vitro effect of plasmin on human platelet function in plasma. Inhibition of aggregation caused by fibrinogenolysis. *Circulation* **85**, 935–941 (1992).
69. Pareti, F. I., Capitanio, A., Mannucci, L., Ponticelli, C. & Mannucci, P. M. Acquired dysfunction due to the circulation of 'exhausted' platelets. *Am. J. Med.* **69**, 235–240 (1980).
70. Guerrero, J. A. et al. Visualizing the von Willebrand factor/glycoprotein Ib–IX axis with a platelet-type von Willebrand disease mutation. *Blood* **114**, 5541–5546 (2009).
71. Casari, C. et al. von Willebrand factor mutation promotes thrombocytopathy by inhibiting integrin αIIbβ3. *J. Clin. Invest.* **123**, 5071–5081 (2013).
72. Andrews, R. K., López, J. & Berndt, M. C. Molecular mechanisms of platelet adhesion and activation. *Int. J. Biochem. Cell Biol.* **29**, 91–105 (1997).
73. Chen, Y. et al. An integrin αIIbβ3 intermediate affinity state mediates biomechanical platelet aggregation. *Nat. Mater.* **18**, 760–769 (2019).
74. Daniel, J. & Tuszynski, G. in *Hemostasis and Thrombosis: Basic Principles and Clinical Practice* 569–573 (JB Lippincott, 1994).
75. Oshinowo, O. T., Copeland, R., Bennett, C. M., Lam, W. A. & Myers, D. R. Platelet contraction force as a biophysical biomarker for bleeding risk in patients with immune thrombocytopenia. *Blood* **132**, 517 (2018).

76. Wang, T. Y. et al. Cluster-randomized clinical trial examining the impact of platelet function testing on practice: the treatment with adenosine diphosphate receptor inhibitors: longitudinal assessment of treatment patterns and events after acute coronary syndrome prospective open label antiplatelet therapy study. *Circ. Cardiovasc. Interv.* **8**, e001712 (2015).
77. Feghhi, S. et al. Glycoprotein Ib–IX–V complex transmits cytoskeletal forces that enhance platelet adhesion. *Biophys. J.* **111**, 601–608 (2016).
78. Lee, J., Leonard, M., Oliver, T., Ishihara, A. & Jacobson, K. Traction forces generated by locomoting keratocytes. *J. Cell Biol.* **127**, 1957–1964 (1994).
79. Liu, Y. et al. DNA-based nanoparticle tension sensors reveal that T-cell receptors transmit defined pN forces to their antigens for enhanced fidelity. *Proc. Natl Acad. Sci. USA* **113**, 5610–5615 (2016).
80. Ma, R. et al. DNA tension probes to map the transient piconewton receptor forces by immune cells. *J. Vis. Exp* **20**, e62348 (2021).
81. Gurbel, P. A. et al. First report of the point-of-care TEG: a technical validation study of the TEG-6S system. *Platelets* **27**, 642–649 (2016).

Acknowledgements

We acknowledge support from NIH 5R01GM131099-04 (K.S.), NIH RM1GM145394 (K.S.) and NSF DMR 1905947 (K.S.). Y.D. is supported by an American Heart Association postdoctoral fellowship (23POST1028975). R.S. acknowledges support from Emory University Department of Anaesthesiology (internal funds). We thank the Emory Mass Spectrometry Center and F. Strobel and H. Ogasawara for ESI–mass spectrometry measurement to validate oligonucleotides. We also thank L. Downey and C. Maier for helpful discussions.

Author contributions

Y.D. and K.S. conceived the project. Y.D. designed experiments, analysed data and compiled the figures. F.S. helped with TEG, aggregometry experiments and related discussions. Y.H., W.C. and R.L. helped with platelet purification and related discussion. Y.K. helped with the design of the experiments. F.S. and R.S. helped design the clinical studies and obtained related samples. Y.D. and K.S. wrote the manuscript. All authors contributed to revising the manuscript.

Competing interests

Y.D., Y.K., R.S. and K.S. are the inventors of a patent application (US Application No. 63/417,239). The remaining authors declare no competing interests.

Additional information

Extended data is available for this paper at https://doi.org/10.1038/s41551-023-01114-1.

Supplementary information The online version contains supplementary material available at https://doi.org/10.1038/s41551-023-01114-1.

Correspondence and requests for materials should be addressed to Roman Sniecinski or Khalid Salaita.

Peer review information *Nature Biomedical Engineering* thanks Yunfeng Chen and the other, anonymous, reviewer(s) for their contribution to the peer review of this work. Peer reviewer reports are available.

https://doi.org/10.1038/s41551-023-01114-1

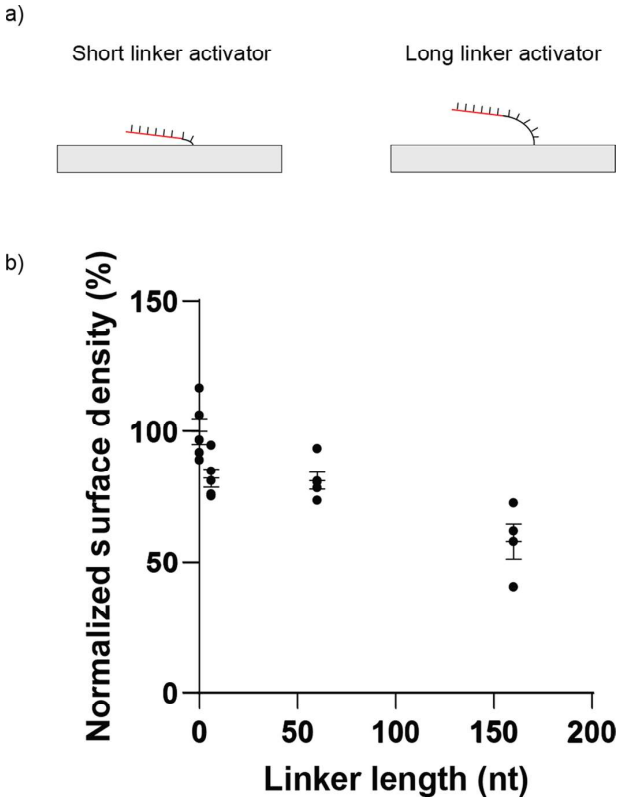

Extended Data Fig. 1 | Comparison of surface density as function of linker length. a) Scheme showing surface tethered activator sequences with different linker lengths. **b**) Plot of normalized surface density as a function of linker length. All biotinylated activators were incubated on streptavidin modified surfaces for 1hr at 100nM. Surface density was determined using fluorescence microscopy of fluorescently tagged activators and normalized to the activator density without linker. Error bar represents S.E.M from five independent surfaces.

https://doi.org/10.1038/s41551-023-01114-1

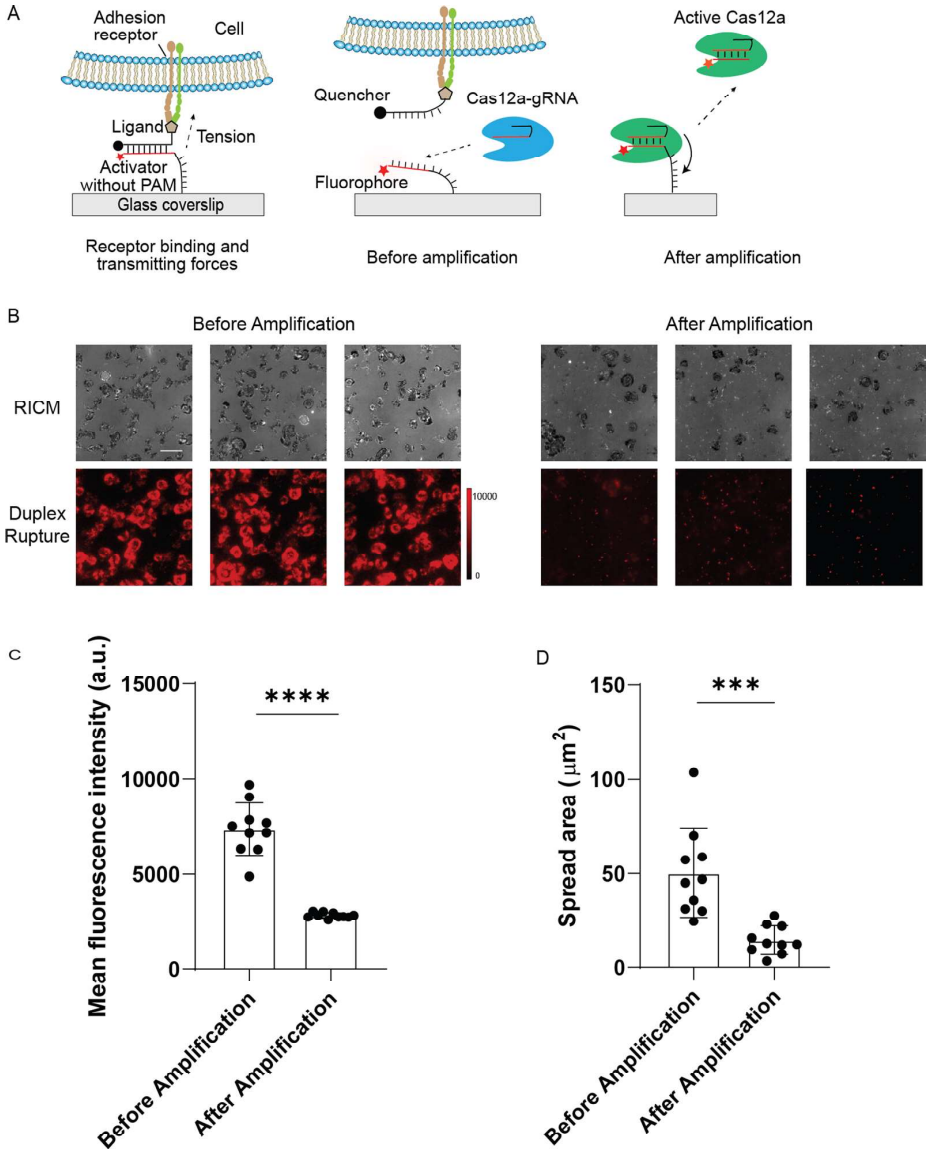

Extended Data Fig. 2 | Cas12a auto-cleavage of surface-tethered activator. **a**) Schematic showing the MCATS process. Molecular traction forces mechanically melt the duplex probe and reveal an activator sequence that triggers Cas12a to cleave the linker of immobilized activators. **b**) Representative RICM, and duplex rupture (red) fluorescence images after platelets were incubated on concealed activator surface. Imaging was initiated after 1 hr after seeding platelets. The images compare the RICM cell spread area and duplex rupture signal before and after Cas12a/gRNA and reporter DNA were added for 1hr. Scale bar = 12 μm. **c**) Plot of mean fluorescence intensity beneath individual platelet before and after amplification. Center for the error bars is the mean fluorescence intensity under 10 individual platelets. Values are raw levels and were not background subtracted. Error bar represents S.D from 10 individual platelets. The p value is calculated by two-sided student *t* test. $p<0.0001$. **d**) Plot of spread area beneath individual platelets determined from RICM before and after amplification. Significance is calculated with two-sided student *t* test, $p = 0.0002$. Error bar represents S.D from 10 individual platelets.

https://doi.org/10.1038/s41551-023-01114-1

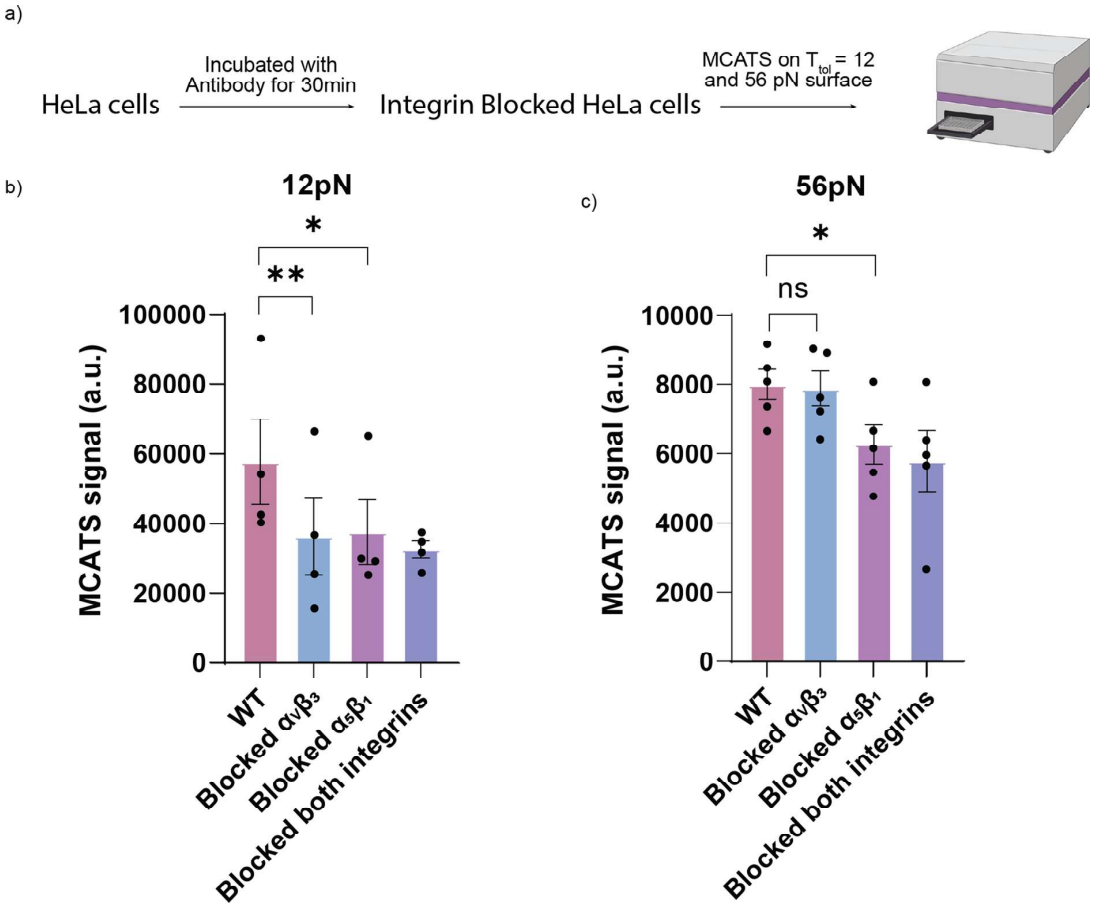

Extended Data Fig. 3 | Integrin subtype inhibition assay with MCATS. **a**) Scheme showing the workflow of how the integrin inhibition assay was performed with MCATS. **b-c**) MCATS results of HeLa cell traction forces inhibited by different integrin monoclonal antibodies. Error bars represent standard error of the mean from n = 4 (T_{tol} = 12pN, panel b) and n = 5 (T_{tol} = 56pN, panel c) independent experiments. Significance is calculated by paired two-tailed t-test.

https://doi.org/10.1038/s41551-023-01114-1

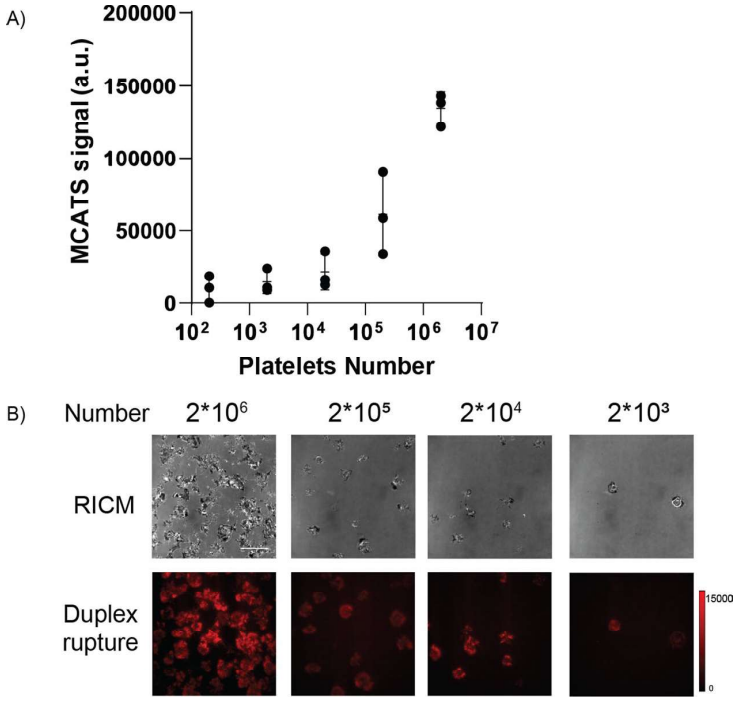

Extended Data Fig. 4 | Measuring MCATS signal as a function of platelet number seeded on a surface. a) Plot of MCATS signal as a function of seeded platelet number. Error bar represents SEM from n = 3 independent experiments **b**) Representative of RICM, duplex rupture (red) fluorescence images and bright field images of tension signal when seeding different number of cells on concealed activator surface. Scale bar = 10 µm.

https://doi.org/10.1038/s41551-023-01114-1

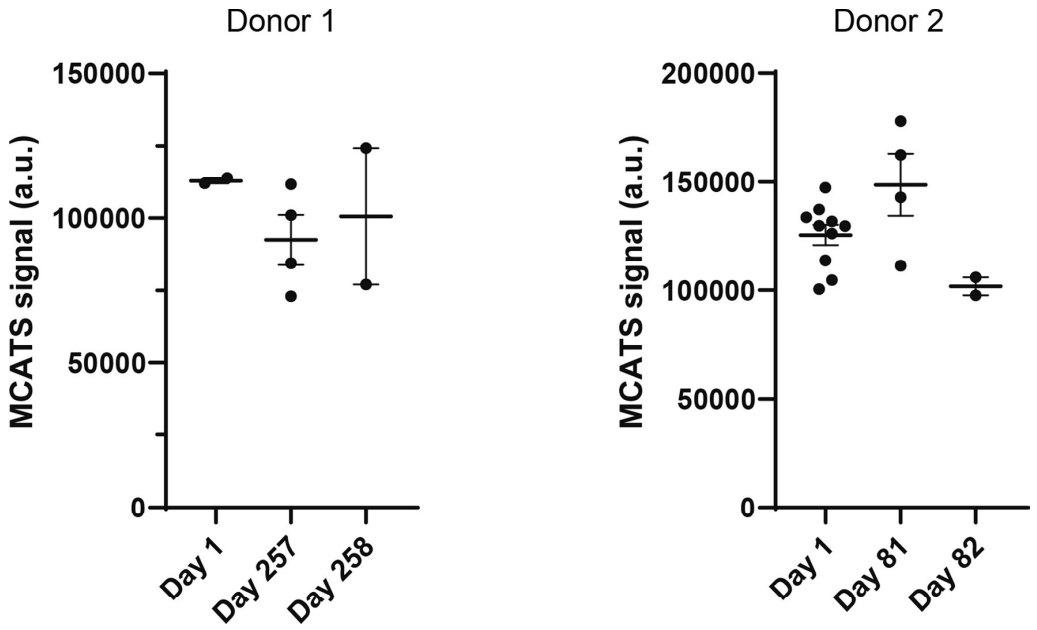

Extended Data Fig. 5 | Day-to-day variance of platelet tension test. a) MCATS results of two healthy donors' platelet tension signal from three individual blood draws performed on separate days. Center of error bar represents average of the measurements. Error bar represents S.D. from n = 2, 4, 2 for donor 1 on different days and 10, 4, 2 for donor 2 at different days.

https://doi.org/10.1038/s41551-023-01114-1

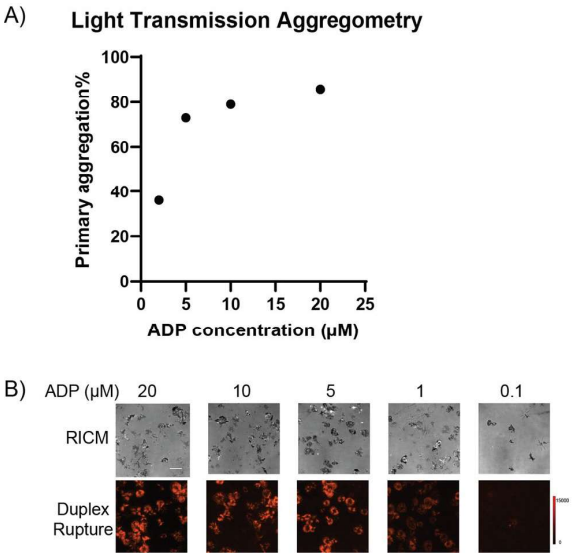

Extended Data Fig. 6 | LTA data for platelet treated with different ADP agonist concentrations. a) Plot showing LTA signal of primary aggregation for platelets treated with ADP. LTA was accomplished using PAP-8E profiler prewarmed to 37 °C. The blank (0% aggregation) was set with PPP. **b**) Representative RICM, duplex rupture fluorescence (red) images for one donor washed platelets that were treated with ADP with concentrations ranging from 0.1 mM to 20 mM. Scale bar = 10 μm. MCATS signal for this data is shown in main Fig. 3.

https://doi.org/10.1038/s41551-023-01114-1

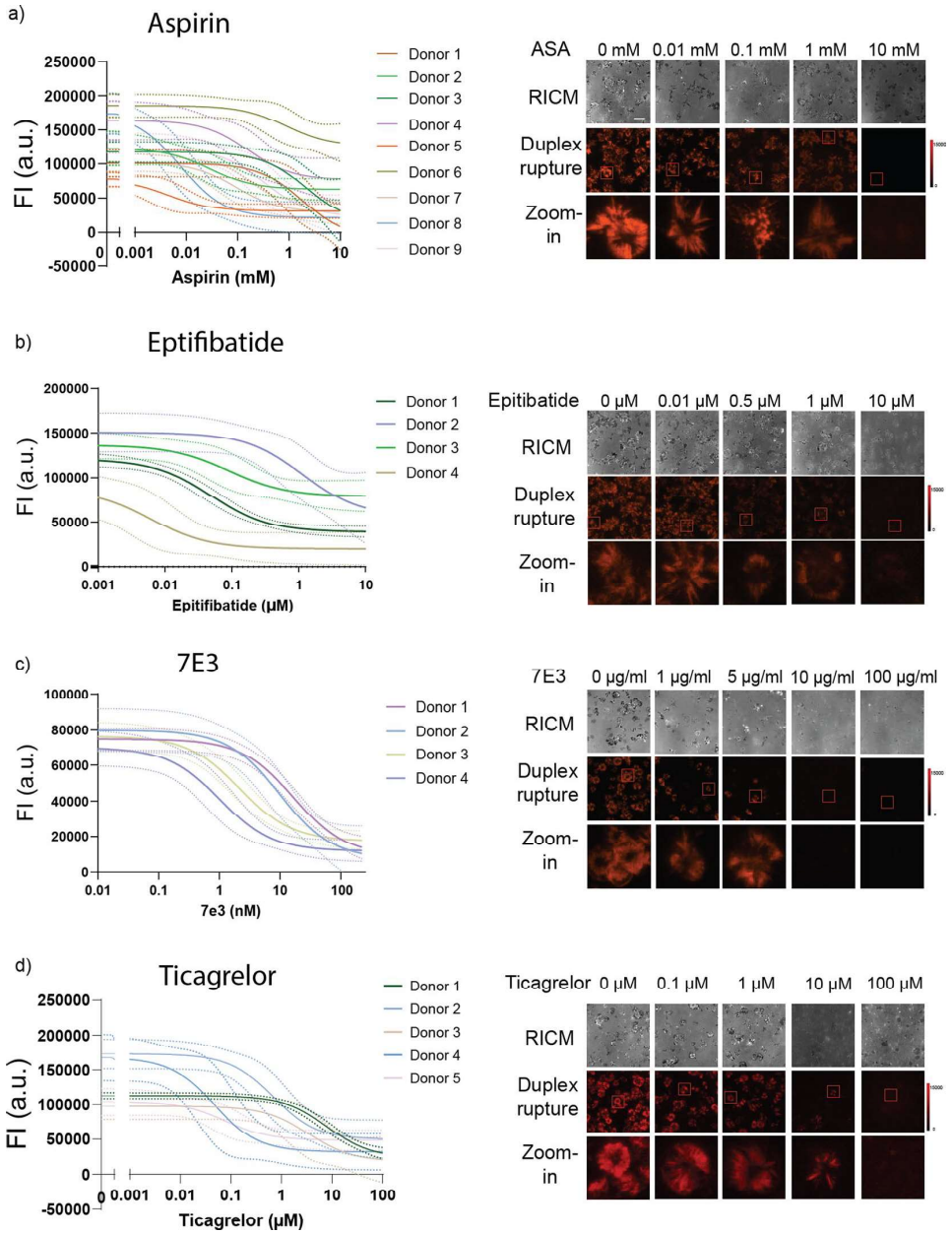

Extended Data Fig. 7 | MCATS measures dose-response curves for platelet inhibitors. a–d) Plots of [Aspirin], [Eptifibatide], [7E3], [Ticagrelor] vs MCATS signal for different donors. A dose-response titration of six drug concentrations for each drug for individual donors is measured with MCATS and all measurements were performed in duplicate or triplicate. Mechano-IC50 for each donor was calculated by fitting plot to a standard dose-response function: Signal = Bottom + (Top-Bottom)/(1+([drug]/IC50). Solid line represents the fitting and dashed line represents 95% CI. Representative RICM, duplex rupture fluorescence (red) and zoom-in fluorescence images for one donor with drug concentrations ranging from 0 mM to 10 mM. Scale bar = 10 μm.

https://doi.org/10.1038/s41551-023-01114-1

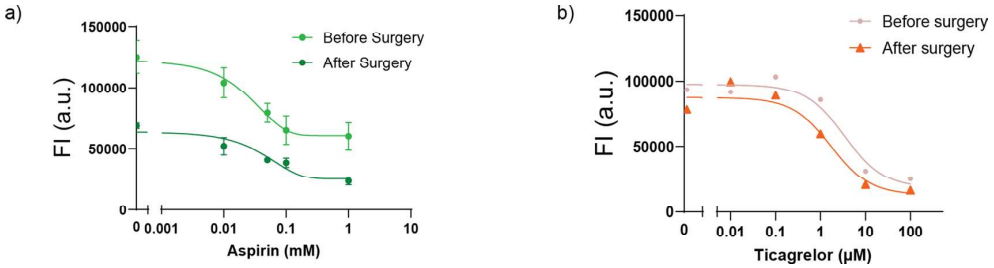

Extended Data Fig. 8 | Sensitivity of aspirin and ticagrelor for patients before and after surgery. a) Plots of [Aspirin] vs MCATS signal for patients before and after surgery. Error bars represent mean and SD from three replicate wells. Center of error bar represents average of the three measurements. Mechano-IC50 for each donor was calculated by fitting plot to a standard dose-response function: Signal = Bottom + (Top-Bottom)/(1+([drug]/IC50). The difference of calculated IC_{50} before and after surgery for two patients is non-significant with two tailed student t test, $P = 0.65$. **b**) Plots of [Ticagrelor] vs MCATS signal for patient before and after surgery. Mechano-IC50 was calculated by fitting plot to a standard dose-response function: Signal = Bottom + (Top-Bottom)/(1+([drug]/IC50).

https://doi.org/10.1038/s41551-023-01114-1

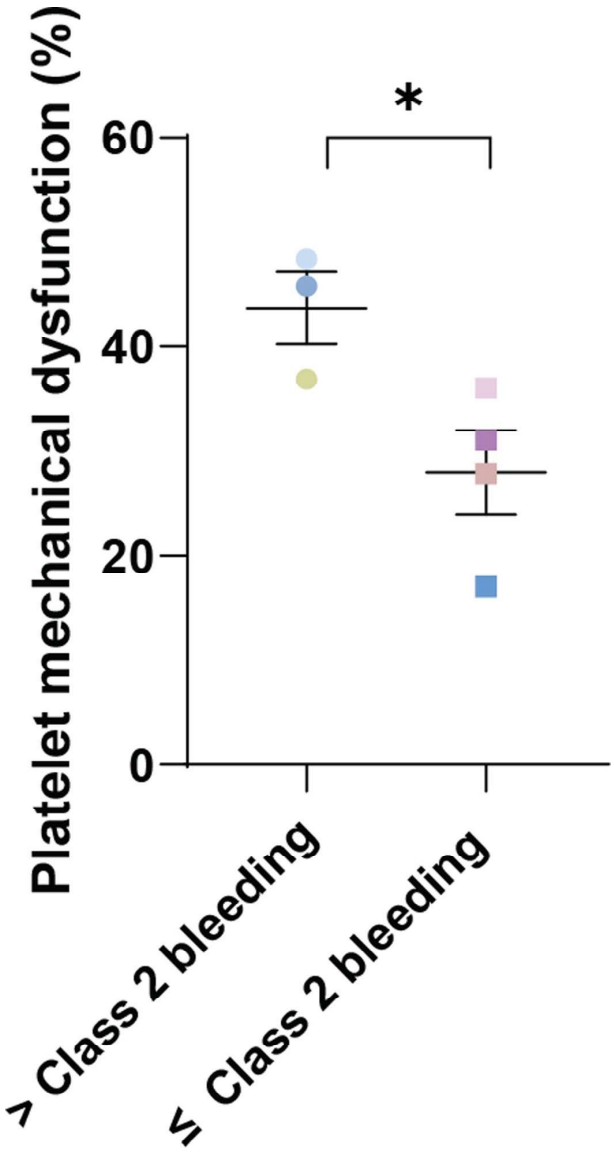

Extended Data Fig. 9 | Patient bleeding severity is correlated with platelet mechanical dysfunction. Plot of reduction in MCATS signal (%) for subjects binned into two groups: mild/insignificant bleeding (class 1 and 2) or moderate/severe/massive bleeding (class 3, 4, and 5). Significance is calculated by a two tailed student t-test with P = 0.03. Error bars represent S.E.M. from n = 3 and 4 subjects respectively.

https://doi.org/10.1038/s41551-023-01114-1

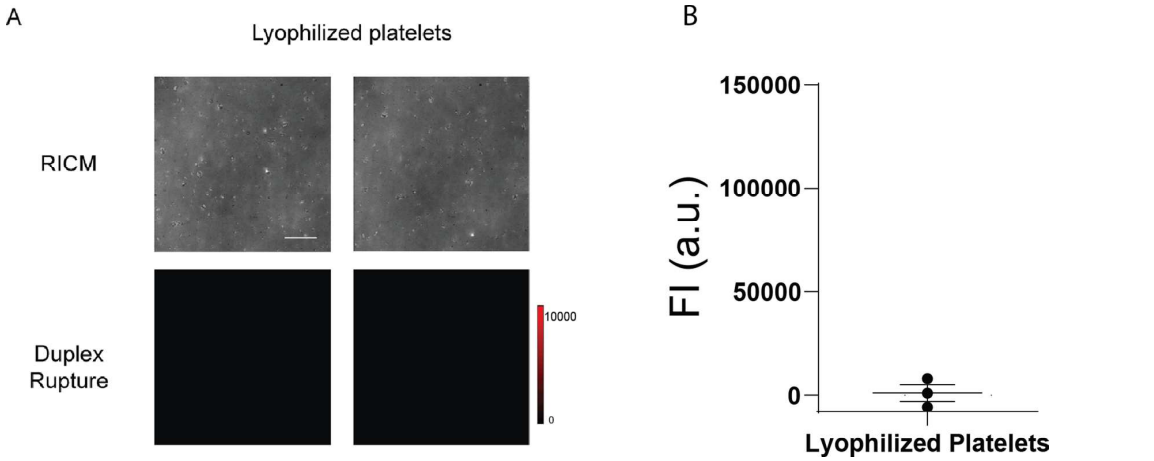

Extended Data Fig. 10 | Tension measurement of lyophilized platelets. **a**) Representative RICM, duplex rupture fluorescence (red) images for lyophilized platelets on tension probes. Scale bar represents 12 μm. **b**) Plot of MCATS signal of lyophilized platelets seeded on concealed DNA tension probes for 1hr. Error bar represents SD from 3 independent wells. Results indicate lyophilized platelets have no active mechanical signal.

nature portfolio

Corresponding author(s): Khalid Salaita

Last updated by author(s): Jun 6, 2023

Reporting Summary

Nature Portfolio wishes to improve the reproducibility of the work that we publish. This form provides structure for consistency and transparency in reporting. For further information on Nature Portfolio policies, see our Editorial Policies and the Editorial Policy Checklist.

Statistics

For all statistical analyses, confirm that the following items are present in the figure legend, table legend, main text, or Methods section.

n/a	Confirmed	
☐	☒	The exact sample size (*n*) for each experimental group/condition, given as a discrete number and unit of measurement
☐	☒	A statement on whether measurements were taken from distinct samples or whether the same sample was measured repeatedly
☐	☒	The statistical test(s) used AND whether they are one- or two-sided *Only common tests should be described solely by name; describe more complex techniques in the Methods section.*
☒	☐	A description of all covariates tested
☐	☒	A description of any assumptions or corrections, such as tests of normality and adjustment for multiple comparisons
☐	☒	A full description of the statistical parameters including central tendency (e.g. means) or other basic estimates (e.g. regression coefficient) AND variation (e.g. standard deviation) or associated estimates of uncertainty (e.g. confidence intervals)
☐	☒	For null hypothesis testing, the test statistic (e.g. *F*, *t*, *r*) with confidence intervals, effect sizes, degrees of freedom and *P* value noted *Give P values as exact values whenever suitable.*
☒	☐	For Bayesian analysis, information on the choice of priors and Markov chain Monte Carlo settings
☒	☐	For hierarchical and complex designs, identification of the appropriate level for tests and full reporting of outcomes
☐	☒	Estimates of effect sizes (e.g. Cohen's *d*, Pearson's *r*), indicating how they were calculated

Our web collection on statistics for biologists contains articles on many of the points above.

Software and code

Policy information about availability of computer code

Data collection	Data from the plate reader was collected with Biotek Gen5 3.05 software. Data from the microscope images were collected with Nikon NIS-Elements 5.30.05 software.
Data analysis	Image analysis was conducted using ImageJ 1.53t. All statistical-significance calculations (p-values), linear regression, correlation analysis r, and dose–response curve fitting were done with Graphpad prism 8.

For manuscripts utilizing custom algorithms or software that are central to the research but not yet described in published literature, software must be made available to editors and reviewers. We strongly encourage code deposition in a community repository (e.g. GitHub). See the Nature Portfolio guidelines for submitting code & software for further information.

Data

Policy information about availability of data

All manuscripts must include a data availability statement. This statement should provide the following information, where applicable:

- Accession codes, unique identifiers, or web links for publicly available datasets
- A description of any restrictions on data availability
- For clinical datasets or third party data, please ensure that the statement adheres to our policy

The data supporting the results in this study are available within the paper and its Supplementary Information. Source data are provided with this paper. Raw data

and images were deposited in Dataverse and can be accessed via the identifier https://doi.org/10.15139/S3/4Q8H1A. All raw and analysed datasets are available from the corresponding author on request. No identifiable information from the participants will be disclosed.

Human research participants

Policy information about studies involving human research participants and Sex and Gender in Research.

Reporting on sex and gender	Sex was not considered as a biological variable in this study. We tried to recruit equal numbers of male and female participants, and sex information is provided in Supplementary Table 3.
Population characteristics	Donor characteristics, including age, are provided in Supplementary Table 3.
Recruitment	Healthy participants were recruited from Emory's campus through advertisement by posted notices and word of mouth. The participants were offered $20 compensation for their time. The cardiopulmonary by-pass donors were recruited during the assessment prior to surgery. Written consent was obtained for all human participants. There were no self-selection biases or other biases.
Ethics oversight	Emory University Ethics Committee, IRB00117177.

Note that full information on the approval of the study protocol must also be provided in the manuscript.

Field-specific reporting

Please select the one below that is the best fit for your research. If you are not sure, read the appropriate sections before making your selection.

☒ Life sciences ☐ Behavioural & social sciences ☐ Ecological, evolutionary & environmental sciences

For a reference copy of the document with all sections, see nature.com/documents/nr-reporting-summary-flat.pdf

Life sciences study design

All studies must disclose on these points even when the disclosure is negative.

Sample size	A minimum of biological triplicates were conducted for all experiments involving cell lines. No predetermination of sample size was performed for the cell-line experiments because significant differences were observed in a two-sided t-test after three experiments. Samples from human participants were collected on the basis of availability, with a minimum sample size of 4. The number of participants enrolled represents a convenience sample, reflecting the number of participants that could be feasibly enrolled within the timeframe and budget of the study.
Data exclusions	Data from defective surfaces or well plates that with a failed positive or negative control were excluded.
Replication	All findings were done with triplicates to confirm reproducibility. All attempts at replication were successful.
Randomization	No treatment group was involved in the study, and therefore no randomization was conducted.
Blinding	Aggregometry/TEG data and MCATS data were collected by different individuals and in different labs and the results were not discussed. The investigators were blinded to group allocation during data collection and data analysis. The cell-line experiments were not blinded.

Reporting for specific materials, systems and methods

We require information from authors about some types of materials, experimental systems and methods used in many studies. Here, indicate whether each material, system or method listed is relevant to your study. If you are not sure if a list item applies to your research, read the appropriate section before selecting a response.

Materials & experimental systems

n/a	Involved in the study
☐	☒ Antibodies
☐	☒ Eukaryotic cell lines
☒	☐ Palaeontology and archaeology
☒	☐ Animals and other organisms
☒	☐ Clinical data
☒	☐ Dual use research of concern

Methods

n/a	Involved in the study
☒	☐ ChIP-seq
☒	☐ Flow cytometry
☒	☐ MRI-based neuroimaging

Antibodies

Antibodies used	Recombinant Anti-CD41 antibody [7E3 (Abciximab)] from Abcam - Chimeric (ab275976), Lot: GR3422387-2 and diluted to a series of concentration in the IC50 test. Anti-Integrin αVβ3 Antibody(clone LM609, MAB1976, Lot#3863390) used at 1:100 dilution and Anti-Integrin α5β1 Antibody(clone JBS5, MAB1969-I, Lot#3941858) used at 1:50 dilution were purchased from Sigma Aldrich.
Validation	Recombinant Anti-CD41 antibody [7E3 (Abciximab)] was validated by Abcam and the information can be found at https://www.abcam.com/products/primary-antibodies/cd41-antibody-7e3-abciximab-rabbit-igg-chimeric-ab275976.html?productWallTab=ShowAll Anti-Integrin αVβ3 Antibody(clone LM609, MAB1976, Lot#3863390) and Anti-Integrin α5β1 Antibody(clone JBS5, MAB1969-I, Lot#3941858) was validated by Sigma Aldrich. And the information can be found at https://www.emdmillipore.com/US/en/product/Anti-Integrin-V3-Antibody-clone-LM609,MM_NF-MAB1976#documentation and https://www.emdmillipore.com/US/en/product/Anti-Integrin-51-Antibody-clone-JBS5,MM_NF-MAB1969-I-100UL#documentation.

Eukaryotic cell lines

Policy information about cell lines and Sex and Gender in Research

Cell line source(s)	NIH/3T3 and HeLa cells were purchased from ATCC.
Authentication	The cell line was not authenticated.
Mycoplasma contamination	All cell lines tested negative for mycoplasma contamination.
Commonly misidentified lines (See ICLAC register)	No commonly misidentified cell lines were used.